False discovery rates of *qpAdm*-based screens for genetic admixture

Eren Yüncü[1,*,†], Ulaş Işıldak[1,*,†], Matthew P. Williams[2], Christian D. Huber[2], Leonid A. Vyazov[1], Piya Changmai[1], Pavel Flegontov[1,3,§]

[1] Department of Biology and Ecology, Faculty of Science, University of Ostrava, Ostrava, Czechia

[2] Department of Biology, Eberly College of Science, Pennsylvania State University, PA, USA

[3] Department of Human Evolutionary Biology, Harvard University, Cambridge, MA, USA

* the authors contributed equally

† present addresses: E.Y., Department of Biological Sciences, Middle East Technical University, Ankara, Turkey; U.I., Leibniz Institute on Aging - Fritz Lipmann Institute (FLI), Jena, Germany.

§ Correspondence to: Pavel Flegontov

(pavel.flegontov@osu.cz, pavel_flegontov@hms.harvard.edu)

Abstract

Although a broad range of methods exists for reconstructing population history from genome-wide single nucleotide polymorphism data, just a few methods gained popularity in archaeogenetics: principal component analysis (PCA); *ADMIXTURE*, an algorithm that models individuals as mixtures of multiple ancestral sources represented by actual or inferred populations; formal tests for admixture such as f_3-statistics and *D*-statistics; and *qpAdm*, a tool for fitting two-component and more complex admixture models to groups or individuals. Despite their popularity in archaeogenetics, which is explained by modest computational requirements and ability to analyse data of various types and qualities, protocols relying on *qpAdm* that screen numerous alternative models of varying complexity and find "fitting" models (often considering both estimated admixture proportions and *p*-values as a composite criterion of model fit) remain untested on complex simulated population histories in the form of admixture graphs of random topology. We analysed genotype data extracted from such simulations and tested various types of high-throughput *qpAdm* protocols ("rotating" and "non-rotating", with or without temporal stratification of target groups and proxy ancestry sources, with or without a "model competition" step). We caution that these *qpAdm* protocols may be inappropriate for exploratory analyses in poorly studied regions/periods since their false discovery rates varied between 12% and 68% depending on the details of the protocol and on the amount and quality of simulated data (i.e., >12% of fitting two-way admixture models imply gene flows that were not simulated), although our study has a number of limitations. We demonstrate that for reducing false discovery rates of *qpAdm* protocols to nearly 0% it is advisable to use large SNP sets with low missing data rates, the rotating *qpAdm* protocol with a strictly enforced rule that target groups do not pre-date their proxy sources, and an unsupervised *ADMIXTURE* analysis as a way to verify feasible *qpAdm* models.

Introduction

Although a broad range of methods exists for reconstructing population history from genome-wide autosomal single nucleotide polymorphism (SNP) data, just a few methods became the cornerstone of archaeogenetic studies: principal component analysis (PCA) (Patterson et al. 2006); an unsupervised or supervised algorithm for admixture inference in individuals, *ADMIXTURE* (Alexander et al. 2009); formal tests for admixture such as f_3-statistics (Patterson et al. 2012, Peter 2016, Soraggi and Wiuf 2019) and *D*-statistics (Green et al. 2010, Durand et al. 2011); and a tool for fitting two-component and more complex admixture models to populations, *qpAdm* (Haak et al. 2015, Harney et al. 2021). The popularity of these methods is explained by their relatively modest computational requirements and versatility since they are capable of analysing unphased biallelic genotype data of various types (pseudo-haploid or diploid), generated using either targeted enrichment on a panel of sites or shotgun sequencing technologies, and low-coverage ancient genomes with high proportions of missing data (Harney et al. 2021). However, only a few studies were devoted to testing the performance of these diverse methods on simulated genetic data (Alexander et al. 2009, Harney et al. 2021, Lazaridis et al. 2017, Martin et al. 2014, McVean 2009, Moreno-Mayar et al. 2018b, Ning et al. 2020, Soraggi and Wiuf 2019), and realistically complex population histories remain virtually unexplored in this respect.

In a typical archaeogenetic study published since the 2010s, PCA is used as a first line of analysis, providing an overview of population structure and helping to propose hypotheses about migration and admixture. Distribution of individual genomes in two- or higher dimensional spaces of principal components (PCs) does not have an unambiguous interpretation since even under ideal conditions (in the absence of missing data, batch artefacts, and selection signals) it is affected by both genetic drift and admixture (McVean 2009). Nevertheless, if context information such as geographical coordinates and dates for ancient individuals is available, PCA is routinely used for revealing “genetic clines” interpreted as signs of admixture between originally isolated groups at the ends of such clines. However, a study on simulated data by Novembre and Stephens (2008) concluded that clinal PCA patterns do not necessarily indicate historical migration events; these patterns generally emerge because of decrease in genetic similarity with distance. PC1 vs. PC2 scatterplots were

also shown to display an arch-shaped artefact, a "horseshoe" (Podani and Miklós 2002), under the homogeneous migration scenario (Novembre and Stephens 2008, Frichot et al. 2012). It was demonstrated that the distribution of individuals in the PC space depends on the expected coalescent time (McVean 2009), hence distinct demographic models with the same expected coalescence times are expected to have the same PCA projections. Additionally, imbalanced sampling across genetically divergent populations affects PCA results substantially (McVean 2009). Hence, using further methods to correlate PCA results with other lines of evidence is necessary for studying migration history (Reich et al. 2008).

Formal tests for genetic admixture such as f_3-statistics and D/f_4-statistics are often used exactly for this purpose: to prove that a certain cline spotted in PC space is a result of migration and admixture of previously isolated ancestries and does not reflect isolation by distance or recurrent bottlenecks. *D*- and f_4-statistics, which are identical except for the denominator and are not affected by genetic drift, test if an unrooted four-population tree fits the data (Reich et al. 2009, Green et al. 2010, Durand et al. 2011, Patterson et al. 2012). A statistically significant deviation of the statistic from 0 (estimated using jackknife or bootstrap resampling) means that either the assumed tree topology is wrong, or gene flow occurred between a pair of branches in the tree, assuming that recurrent mutations and SNP ascertainment bias are absent (Durand et al. 2011, Patterson et al. 2012). However, interpretation of these statistics is ambiguous since gene flow directionality remains unknown, and two pairs of branches can be responsible for a deviation of the statistic from 0 (Lipson 2020). Since gene flow may be mediated by ghost groups related only distantly to the sampled groups at the branch tips (Tricou et al. 2022), excluding one pair of branches due to geographical and temporal plausibility of gene flow is also difficult. And interpretation of deviations of *D*- and f_4-statistics from 0 becomes hardly possible if both branch pairs are connected by detectable gene flows.

"Admixture" f_3-statistics of the form f_3(target; proxy source$_1$, proxy source$_2$) constitute another formal test for admixture (Patterson et al. 2012). Significant deviation of such a statistic from 0 in the negative direction (Z-score below -3) is considered proof of admixture since allele frequencies at most sites are intermediate in the target group between those in the proxy sources (Patterson et al. 2012). However, "admixture" f_3-statistics are usually only applicable for detection of recent admixture events since they become positive when post-

104 admixture genetic drift on the target lineage moves allele frequencies away from these
105 intermediate values (Patterson et al. 2012, Peter 2016).

106 Considering these complications, more sophisticated tests for genetic admixture are needed.
107 The *qpAdm* method introduced by Haak *et al*. (2015) is based on matrices of f_4-statistics and
108 does not require detailed knowledge of population phylogeny beyond a few assumptions
109 (Lazaridis et al. 2016, Harney et al. 2021). This method tests admixture models in the form of
110 combinations of proxy ancestral groups ("sources" or "references", Lazaridis et al. 2016) for
111 a "target" (or "test") population, given a genetically diverse set of "outgroup" populations,
112 and infers ancestry proportions in the target group contributed by the lineages represented
113 by the proxy sources ("outgroups" are often termed "right" populations for convenience since
114 they are usually not outgroups in the phylogenetic sense, and they were termed "references"
115 by Harney *et al*. 2021). See Box 1 for definitions of various *qpAdm*-related terms.

116 **Box 1.** Terminology used in this study for describing admixture models, results of screens for
117 admixture, and *qpAdm* protocols.

"right" (or outgroup) populations/groups	In a *qpAdm* protocol, these are reference populations needed for testing admixture models composed of a target and one or several proxy source groups.
target (or test) population/group	In an admixture model, this is a population/group whose genetic history is being modelled.
true (ancestry) source	In the context of simulated admixture graphs, this is a population directly participating in an admixture event(s) giving rise to a target group, and its ancestral (unsampled) population before its merging with other populations.
proxy (ancestry) source	In the context of simulated admixture graphs, this is a sampled population included in an admixture model as a potential source and assumed to be cladal with one of true ancestry sources.
model complexity	Number of proposed proxy ancestry sources in an admixture model "target = proxy source$_1$ + proxy source$_2$ + … proxy source$_i$".
"left" populations/groups	In a *qpAdm* model, these are proxy sources and a target.
reference populations/groups	"Right" and proxy source populations combined.
(composite) model feasibility criterion	A criterion for identifying fitting (feasible) *qpAdm* models that relies on both estimated admixture proportions and the *p*-value. The following criterion was used in this study (all the conditions listed below should be satisfied): 1) *p*-values for all models with *n–1* ancestry sources, such as one-way models "target = proxy

	source$_1$", "target = proxy source$_2$", and "proxy source$_1$ = proxy source$_2$", are all below 0.01; 2) for a model with *n* ancestry sources, such as a two-way model "target = proxy source$_1$ + proxy source$_2$", estimated admixture proportions $\pm$ 2 standard errors are between 0 and 1; 3) the *p*-value for a model with *n* ancestry sources $\geq$ 0.01. Other versions of this criterion are also found in the literature: with different values of the *p*-value cut-off and/or not considering standard errors of estimated admixture proportions.
feasible (or fitting) *qpAdm* model	A *qpAdm* model satisfying the feasibility criterion above.
positive/negative admixture model	An admixture model supported/not supported by one or several analytical tools such as *qpAdm*, PCA, *ADMIXTURE*.
false discovery rate (FDR)	The fraction of admixture models of a certain complexity (e.g., two-way) satisfying the *qpAdm* model feasibility criteria but classified as false considering the simulated graph topology and simulated admixture proportions. For topological criteria used for classifying two-way admixture models into true and false ones see the Results and Methods sections. The term is also applied to outcomes of more complex admixture inference pipelines composed of several methods.
false omission rate (FOR)	The fraction of feasible *qpAdm* models that are classified as true considering the simulated graph topology and simulated admixture proportions but are not supported by another method (*qpAdm* model competition, PCA, or *ADMIXTURE*) or a combination of methods.
“rotating” *qpAdm* protocol	A protocol having the following feature: a large subset of reference populations or all of them are distributed between the “right” and “left” sets according to the principle “whatever is not in the left set is in the right set”, testing all possible bisections of this sort for a given rotated set and a given range of model complexities. In the most extreme case, target groups are also included in this rotation. Model testing starts from the simplest one-way models and moves on to the next complexity level if all simple models for a given target are rejected according to the composite feasibility criterion. The goal of this approach, as compared to “non-rotating” protocols, is to increase the power of the method to reject non-optimal proxy ancestry sources.
“non-rotating” *qpAdm* protocol	This protocol we also term “standard” or “basic”: all models are tested with one or few fixed sets of “right” groups which usually pre-date “left” groups or are contemporaneous with them. In practice, modern populations genetically divergent from the target are often included in such a “right” set if ancient reference groups are unavailable. Model testing starts from the simplest one-way models and moves on to the next complexity level if all

	simple models for a given target are rejected according to the composite feasibility criterion.
temporal stratification of targets and proxy sources	A requirement that target groups post-date or are contemporaneous with all proxy sources in each model. In practice, this requirement is often included in rotating and non-rotating *qpAdm* protocols.
"distal" *qpAdm* protocol	A rotating or non-rotating *qpAdm* protocol with temporal stratification of targets and proxy sources.
"proximal" *qpAdm* protocol	A rotating or non-rotating *qpAdm* protocol without temporal stratification of targets and proxy sources.
model competition	A *qpAdm* protocol which starts from sets of alternative feasible *qpAdm* models of a certain complexity level for a given target, outcomes of a non-rotating protocol. Alternative proxy sources from these models form a rotated set. Rotation can be performed in two ways (groups from the rotated set are placed in the "left" set one by one, and the other groups from the rotated set are placed in the "right" set; or groups from the rotated set are placed in both "left" and "right" sets one by one), and the composite feasibility criterion is applied. The goal of this approach is to increase the power of the method to reject non-optimal proxy ancestry sources.
proximal model competition *qpAdm* protocol	As introduced by Narasimhan *et al*. (2019), this is a non-rotating *qpAdm* protocol with temporal stratification of "right" and "left" sets, with a subsequent model competition step, and with no (or very limited) temporal stratification of targets and proxy sources at both steps.

Eight years later we find *qpAdm*-based protocols routinely employed in large-scale screens of ancient human or animal populations for admixture (often between closely related sources) and used as formal tests for admixture (see Lazaridis et al. 2016, Skoglund et al. 2017, Harney et al. 2018, Mathieson et al. 2018, Antonio et al. 2019, Narasimhan et al. 2019, Fernandes et al. 2020, Marcus et al. 2020, Ning et al. 2020, Wang et al. 2020, Yang et al. 2020, Calhoff et al. 2021, Papac et al. 2021, Librado et al. 2021, Sirak et al. 2021, Wang et al. 2021, Yaka et al. 2021, Zhang et al. 2021, Allentoft et al. 2022, Bergström et al. 2022, Changmai et al. 2022a, Changmai et al. 2022b, Gnecchi-Ruscone et al. 2022, Lazaridis et al. 2022, Maróti et al. 2022, Oliveira et al. 2022, Patterson et al. 2022, Brielle et al. 2023, Lee et al. 2023, Taylor et al. 2023 for examples). *qpAdm* fits admixture models to a matrix of f_4-statistics of the form f_4("left" group$_i$, "left" group$_j$; "right" group$_i$, "right" group$_j$), which in the absence of missing data at

130 the group level can be reduced to a smaller matrix f_4(target group, "left" group$_j$; "right"
131 group$_1$, "right" group$_j$), considering algebraic relationships between different f_4-statistics
132 (Peter 2016).

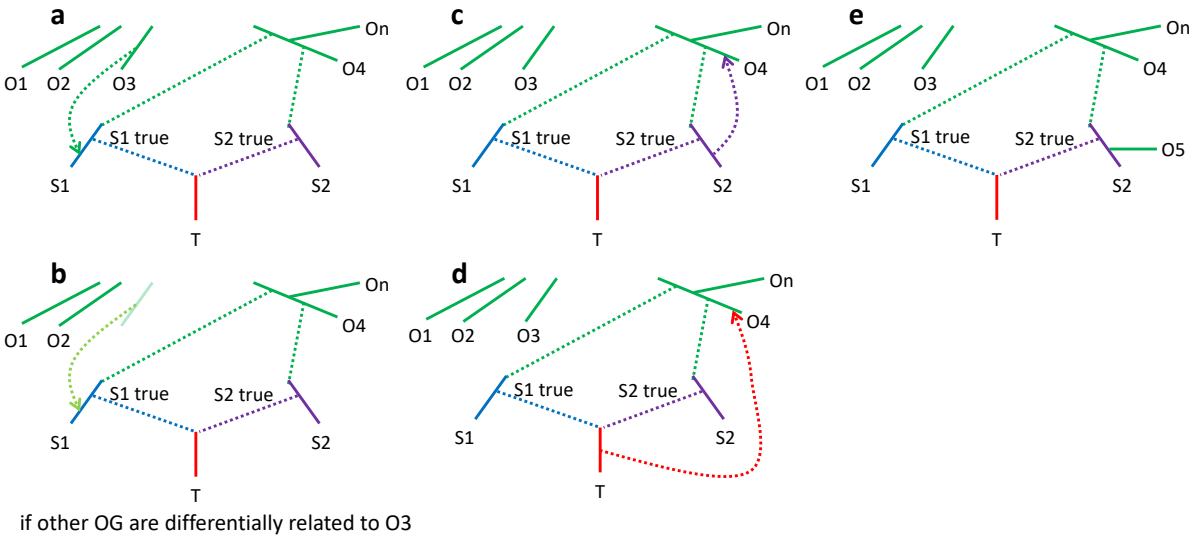

133

134 **Figure 1.** Admixture graphs showing an exhaustive list of assumption violations of the standard *qpAdm*
135 protocol that may lead to rejection of the true simple model, and thus prompt the researcher to test
136 overly complex models. (**a**) A gene flow from an outgroup O* to a proxy source after the divergence
137 of the latter from the true source. (**b**) A gene flow from an unsampled source to a proxy source after
138 the divergence of the latter from the true source. This case is problematic only if the outgroups are
139 differentially related to the unsampled source. (**c**) A gene flow from a proxy source to an outgroup
140 after the divergence of the former from the true source. (**d**) A gene flow from a target to an outgroup.
141 (**e**) An outgroup is cladal with a proxy source.

142

143 A *qpAdm* protocol that has become the standard in archaeogenetics (Lazaridis et al. 2016)
144 can be broken down into two parts: estimation of the number of gene flows connecting the
145 "right" and "left" sets (this method was first published as a tool named "*qpWave*", Reich et
146 al. 2012) and inference of admixture proportions in a target group in the "left" set (Haak et
147 al. 2015). *qpWave* tests for the number of distinct gene flows connecting the "right" and "left"
148 population sets, does not infer directionality of gene flows, and does not identify recipients
149 of gene flow in the "left" or "right" population sets. Notably, the standard *qpAdm* protocol
150 relies on the following assumptions (Lazaridis et al. 2016, Harney et al. 2021): 1) there is at
151 least one "right" population differentially related to the proxy sources; 2) proxy sources are
152 strictly cladal with the true ancestral admixing sources (Fig. 1a,b), 3) there are no gene flows
153 to populations located in the "right" set from the proxy source or target lineages either after

154 the split of the proxy source from the true admixing source population or between the target
155 population and the admixture event that gave rise to it (Fig. 1c-e);. In the context of our study,
156 true sources are unsampled populations that participated in a simulated admixture event
157 (labelled as “S1 true” and “S2 true” in Fig. 1, see also Box 1).

158 If the above assumptions are satisfied, it is safe to say that *qpWave/qpAdm* rejections of
159 simpler models, and a failure to reject more complex models, are the result of a genuinely
160 complex admixture history that connects the source and target populations rather than the
161 false rejection of the simple model due to violations of any one of the assumptions described
162 above. Most notably, violations of the second or third assumptions raise the probability of
163 rejecting a simpler (true) model and prompt the researcher to test more complex (false)
164 models (such as in Fig. 1 rejecting a two-source *qpAdm* model and exploring three-source
165 models).

166 Harney *et al*. (2021) demonstrated on simulated data that, if the *qpAdm* assumptions are
167 satisfied, it is highly favourable for statistical power of the method (for distinguishing
168 between alternative proxy sources that are unequally distant genetically from the true
169 ancestry source) to move at least some alternative proxy sources between the "left" and
170 "right" sets. In other words, having "on the right" populations that do not violate the
171 topological assumptions of *qpAdm*, but are closely related to proxy sources on the "left",
172 increases the statistical power greatly (see also Ning et al. 2020 for another demonstration
173 of this on simple simulated histories).

174 This new type of *qpAdm* protocols, termed "rotating" protocol, has been adopted in
175 archaeogenetics widely (see, e.g., Skoglund et al. 2017, Harney et al. 2019, Narasimhan et al.
176 2019, Olalde et al. 2019, Calhoff et al. 2021, Fernandes et al. 2021, Librado et al. 2021,
177 Allentoft et al. 2022, Bergström et al. 2022, Lazaridis et al. 2022, Oliveira et al. 2022, Taylor
178 et al. 2023). The most extreme version of the "rotating" protocol simply divides a set of
179 reference populations into all possible combinations of "right" and "proxy source" subsets of
180 certain sizes and rotates these combinations through successive *qpAdm* analyses. Additional
181 constraints can be placed on the rotating combinations such as restricting a set of groups
182 (usually highly divergent from the target) to remain in the “right” set in all models. When
183 evaluating the totality of multiple *qpAdm* tests, the simplest feasible models (e.g., one-way,

184 i.e., unadmixed) are favoured, and increasingly complex models are explored upon the
185 rejection of simpler models. Model rejection for the simplest models is made according to a
186 chosen *p*-value threshold such that *qpAdm* models are considered feasible or "fitting" the
187 data when the *p*-value is above such a threshold (Skoglund et al. 2017, Harney et al. 2018,
188 Narasimhan et al. 2019, Olalde et al. 2019, Yang et al. 2020, Calhoff et al. 2021, Fernandes et
189 al. 2021, Librado et al. 2021, Zhang et al. 2021, Allentoft et al. 2022, Bergström et al. 2022,
190 Lazaridis et al. 2022, Oliveira et al. 2022, Taylor et al. 2023). As an additional criterion of a
191 fitting model, all inferred admixture proportions (Harney et al. 2018, Olalde et al. 2019, Yang
192 et al. 2020, Zhang et al. 2021, Allentoft et al. 2022, Lazaridis et al. 2022, Oliveira et al. 2022),
193 or proportions $\pm$ 2 standard errors (Narasimhan et al. 2019), may be required to lie between
194 0 and 1. It is important to remember that the statistical significance of the *qpAdm/qpWave*
195 test is, strictly speaking, a function of model rejection, and thus the failure to reject a model
196 may have underlying causes other than approximating the true situation well enough (such
197 as lack of statistical power or a lack of suitable “right” groups that capture the divergent
198 ancestry sources amongst the “left” group).

199 A less exhaustive version of the rotating *qpAdm* protocol, termed "model competition" (e.g.,
200 Narasimhan et al. 2019, Fernandes et al. 2020, Calhoff et al. 2021, Sirak et al. 2021, Zhang et
201 al. 2021, Maróti et al. 2022, Brielle et al. 2023, Lee et al. 2023), is used even more widely than
202 the basic rotating protocol. It involves an initial (standard non-rotating) *qpAdm* analysis on a
203 number of source populations (see Box 1). Upon identifying a sub-list of plausible sources for
204 a target, the algorithm re-tests feasible models for this target rotating these plausible sources
205 between the "left" and "right" sets with the expectation of improving the power to reject
206 models including proxy sources that are genetically distant from the true sources.

207 The rotating *qpAdm* protocol and model competition are increasingly used as central
208 methods for testing admixture hypotheses proposed after inspecting distributions of
209 individuals in PC spaces, similarity patterns in outcomes of *ADMIXTURE* analyses, and *f/D*-
210 statistics indicative of an admixture graph rather than a simple tree relationship. Yet, the only
211 study reporting detailed testing of *qpAdm* on simulated data (Harney et al. 2021) was
212 performed in extremely favourable conditions: the simulated graph included just two non-
213 nested admixture events; the sources for the principal target group diverged about 1,200

214 generations ago (almost 35,000 years ago in the case of humans); the proxy sources were
215 strictly cladal with the actual ancestral groups for the target; several groups differentially
216 related to these ancestry sources were available; the simulated data were free of
217 ascertainment bias since sites were sampled in a random way; one million sites were used
218 for most analyses; and only 50/50% simulated admixture proportions were tested for some
219 analyses. This study confirmed that the method behaves as expected under these ideal
220 conditions and offered some important guidelines on the choice and number of "right"
221 populations for optimal specificity of the method and on model comparison strategies, and
222 also showed that the results are robust to the presence of missing data, imbalanced group
223 sizes, ancient DNA damage, and to a particular type of SNP ascertainment: selecting sites
224 heterozygous in one individual from a certain population (Patterson et al. 2012). Among
225 challenging historical scenarios, only multifurcation with subsequent continuing gene flow
226 among several groups was explored, and it was concluded that *qpAdm* is not applicable in
227 this case (Harney et al. 2021). Meanwhile, the false discovery rate (FDR) or the false positive
228 rate (FPR) of the method and violations of the topological assumptions of *qpAdm* (Fig. 1)
229 remained virtually unexplored. Thus, the method was proven to work and fail in polar (either
230 extremely favourable or extremely unfavourable) conditions. But what happens in
231 intermediate cases where arguably most of the history of humans and other mammals fits: a
232 history that is not a nearly perfect tree, but that, on the other hand, cannot be represented
233 solely by gene flows homogeneous in space and constant in time?

234 We are concerned that *qpAdm* performance may be compromised by the fact that the
235 topological assumptions of the method are hard to verify in practice, especially the
236 assumption about cladality of proxy and true ancestry sources (i.e., no gene flow to the proxy
237 source population after its split from the true admixing source population). To explore this
238 problem, we analyse simulated population histories in the form of complex random
239 admixture graphs and test various types of *qpAdm* protocols common in the literature:
240 rotating and non-rotating, with or without temporal stratification of target groups and proxy
241 ancestry sources, with or without a model competition step. We also reproduced other
242 aspects of a typical archaeogenetic study on simulated data: we combined various *qpAdm*
243 protocols with PCA and an unsupervised *ADMIXTURE* analysis to explore FDR of complex
244 admixture screening pipelines.

Results

An overview of published rotating and model competition qpAdm protocols

First, we outline two published rotating *qpAdm* protocols (Narasimhan et al. 2019, Lazaridis et al. 2022) that are typical for this class of protocols (see further examples in Skoglund et al. 2017, Harney et al. 2019, Olalde et al. 2019, Calhoff et al. 2021, Fernandes et al. 2021, Librado et al. 2021, Allentoft et al. 2022, Bergström et al. 2022, Oliveira et al. 2022, Taylor et al. 2023). Lazaridis *et al*. relied on the following set of 15 reference populations: 1) Mbuti (present-day Africans); 2) a Palaeolithic group from the Caucasus (CHG, Caucasian hunter-gatherers); 3) East European Mesolithic (EHG, East European hunter-gatherers); 4) Ganj Dareh (a Neolithic group from Iran); 5) Natufians (an Epipalaeolithic group from Israel); 6) a Pre-pottery Neolithic (PPN) group from the Levant; 7) Taforalt (an Epipalaeolithic group from Morocco); 8) Neolithic Mesopotamia; 9) Afontova Gora 3 (an individual from Late Upper Palaeolithic Siberia); 10) Mal'ta 1 (an individual from Late Upper Palaeolithic Siberia); 11) a Mesolithic group from the Iron Gates region (Serbia); 12) Boncuklu (a Pre-pottery Neolithic group from Central Turkey); 13) Barcın (a Neolithic group from Western Turkey); 14) Pınarbaşı (an Epipalaeolithic individual from Turkey); and 15) Mesolithic and Palaeolithic individuals from Western Europe (WHG, West European hunter-gatherers).

This reference set was divided into all possible "right" and proxy source subsets, except for the African group (Mbuti) which stayed in the "right" set in all models. Three Chalcolithic groups from Iran and an Early Bronze Age group from Russia (Yamnaya) were considered as proxy sources only and not rotated to the "right" set, and various clusters of Chalcolithic and Bronze Age individuals (most of them dated between ca. 5000 and 1000 years BCE) from the Balkans, Anatolia, Levant, Caucasus, Mesopotamia, and Iran were target groups for the *qpAdm* analyses. Thus, this protocol can be classified as a distal rotating protocol (Box 1) since most (but not all) targets do not pre-date the proxy sources (Fig. 2a). For each target, progressively more complex admixture models were tested, including from one to five proxy sources, and in most cases only the simplest feasible models were interpreted. Model feasibility criteria were as follows: estimated admixture proportions between 0 and 1, and *p*-value > 0.01. Among alternative models for the same target, those having a higher *p*-value were considered fitting the data better (Lazaridis et al. 2022).

a, Lazaridis *et al*. 2022, distal rotating protocol

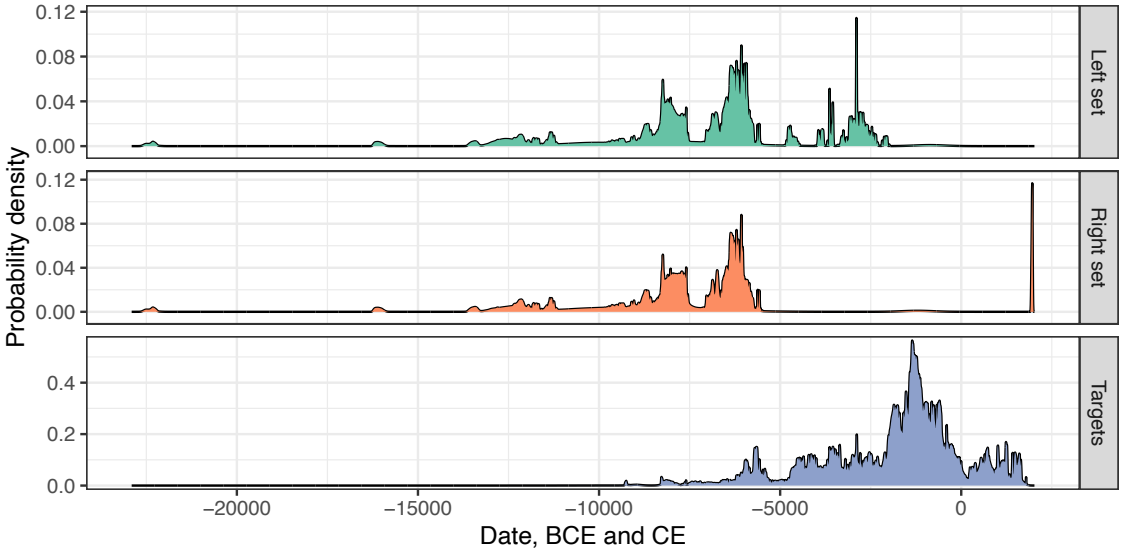

b, Narasimhan *et al*. 2019, distal rotating protocol

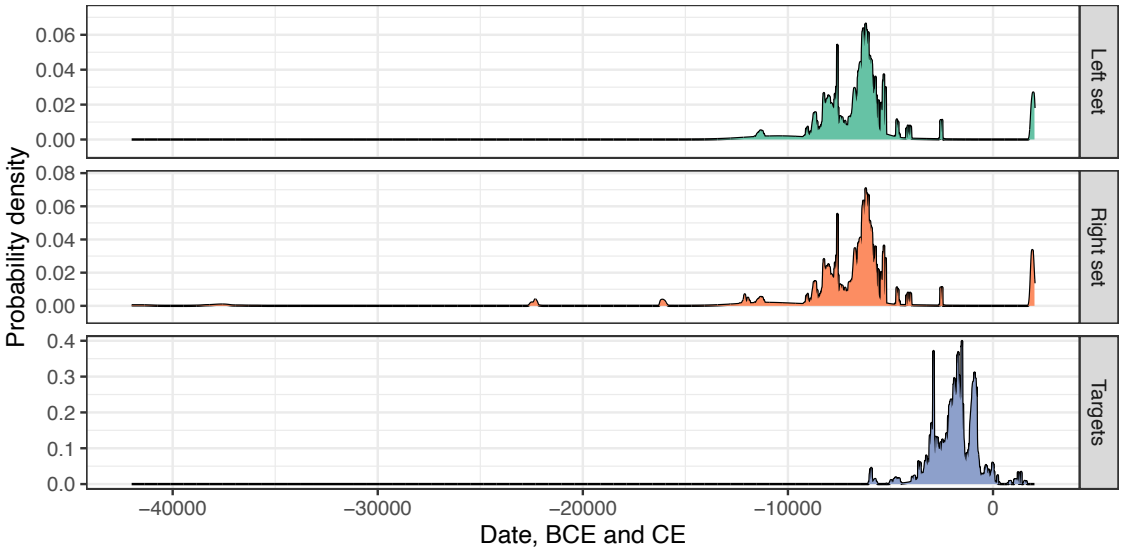

c, Narasimhan *et al*. 2019, proximal model competition protocol

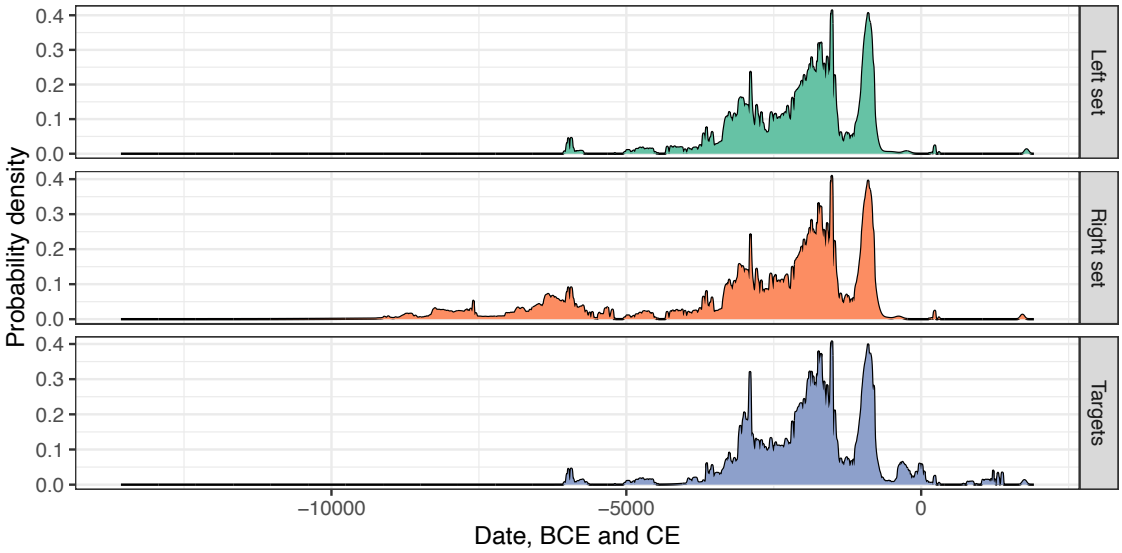

Figure 2. Distributions of radiocarbon and calendar dates for populations sets analyzed with the distal rotating *qpAdm* protocols by Lazaridis *et al*. 2022 (**a**) and Narasimhan *et al*. 2019 (**b**), and with the proximal model competition protocol from Narasimhan *et al*. 2019 (**c**). Probability density curves are shown for three sets of groups: 1) those appearing in the "right" set in at least one *qpAdm* model; 2) those appearing in the "left" set in at least one *qpAdm* model; 3) target groups. Targets in the former study were composed of large clusters of West Eurasian individuals, some of them dating back to the Palaeolithic (Lazaridis et al. 2022). For that reason, the date distribution for targets in panel **a** is very wide.

As shown in Fig. 2a, in this analytical setup there is a large temporal overlap between “left” groups (targets and, on average, earlier proxy sources) and “right” groups. For instance, such a divergent and ancient group as the Mal’ta 1 individual from the vicinity of Lake Baikal (dated to ca. 24,000 years before present, yBP, Raghavan et al. 2014) appeared “on the left” in some *qpAdm* models. Thus, “left-to-right” gene flows (that may lead to erroneous conclusions from a *qpAdm* analysis, see Fig. 1) are expected to be common in the analytical setup used by Lazaridis *et al*.

Narasimhan *et al*. (2019) used both proximal and distal *qpAdm* protocols (Box 1). The distal rotating protocol relied on the following set of 16 reference populations: 1) Mota (a 4500-years-old individual from Ethiopia); 2) Ust’-Ishim (an Upper Palaeolithic individual from West Siberia); 3) Tianyuan (an Upper Palaeolithic individual from Northeast China); 4) Late Upper Palaeolithic individuals from Siberia (Afontova Gora 3 and Mal’ta 1, collectively labelled “ANE” or “Ancient North Eurasians”); 5) a Late Upper Palaeolithic individual from Italy (Villabruna); 6) Natufians (an Epipalaeolithic group from Raqefet, Israel); 7) a Mesolithic individual from Iran (Belt Cave); 8) present-day Andamanese; 9) East European Mesolithic individuals (EEHG, East European hunter-gatherers); 10) West Siberian Mesolithic (WSHG, West Siberian hunter-gatherers); 11) a Pre-pottery Neolithic (PPN) group from the Levant; 12) a Mesolithic group from the Iron Gates region (WEHG, West European hunter-gatherers); 13) Anatolian Neolithic individuals; 14) Ganj Dareh (a Neolithic group from Iran); 15) an Early Neolithic group from the Baikal region (ESHG, East Siberian hunter-gatherers); and 16) present-day Han Chinese. This reference set was split into all possible “right” and proxy source subsets, except for the Upper Palaeolithic individuals/groups (Ust’-Ishim, Tianyuan, ANE, Villabruna) who stayed in the “right” set in all models. Diverse groups from Iran, Pakistan, Central Asia, and the Russian steppe zone (dated from the Chalcolithic to the

314 historical period) were used as targets for the *qpAdm* protocol. For each target, generally
315 post-dating the proxy sources (Fig. 2b), progressively more complex admixture models were
316 tested, from one- to five-way mixture models, and in most cases only the simplest feasible
317 models were interpreted. Model feasibility criteria were as follows: estimated admixture
318 proportions $\pm$ 2 standard errors are between 0 and 1, and *p*-value > 0.01 (Narasimhan et al.
319 2019).

320 In summary, this *qpAdm* protocol rotated a diverse set of groups between the "right" and
321 "left" sets: from present-day to Mesolithic groups older than 10,000 years, and from Africans
322 to South and East Asians (see date distributions in Fig. 2b). Another *qpAdm* protocol used by
323 Narasimhan *et al*., termed "proximal" protocol (Box 1), relied on a smaller fixed set of groups
324 that were kept always "on the right": 1) Mota (a 4500-years-old individual from Ethiopia); 2)
325 East European Mesolithic individuals (EEHG, East European hunter-gatherers); 3) West
326 Siberian Mesolithic (WSHG, West Siberian hunter-gatherers); 4) a Pre-pottery Neolithic (PPN)
327 group from the Levant; 5) a Mesolithic group from the Iron Gates region (WEHG, West
328 European hunter-gatherers); 6) Anatolian Neolithic individuals; 7) Ganj Dareh (a Neolithic
329 group from Iran); 8) an Early Neolithic group from the Baikal region (ESHG, East Siberian
330 hunter-gatherers). Thirty-one diverse Neolithic, Chalcolithic and Bronze Age groups from
331 Eurasia were originally used as proxy sources in one- to three-way models, but if several
332 feasible models were found for the target, the proxy sources from those models were moved
333 one by one from the "left" to the "right" sets (i.e., model competition was performed). The
334 set of targets and the model feasibility criteria matched those for the "distal" protocol. At the
335 model competition step, groups very close in space and time appeared on both sides of the
336 "left" - "right" and proxy source - target divides (Fig. 2c), making “left-to-right” gene flows
337 (Fig. 1) highly likely. Of 45 target groups, 23 groups were also used as rotated proxy sources.
338 For this reason, we interpreted the Narasimhan *et al*. proximal model competition protocol
339 as follows (Box 1): its first step is a non-rotating *qpAdm* protocol with temporal stratification
340 of “right” and “left” sets, but with no (or very limited) temporal stratification of targets and
341 proxy sources; and the second step is a model competition protocol with no (or very limited,
342 see Fig. 2c) temporal stratification of targets and proxy sources. We note that any such
343 interpretation is an approximation that captures most important features of a published
344 protocol and omits some details.

345 Since the sets of groups that are split into the "left" and "right" subsets in the protocols
346 summarized above are very diverse chronologically and genetically, and since there are major
347 overlaps in dates between the "left" and "right" subsets (Fig. 2), we argue that this approach
348 is essentially similar to taking an admixture graph connecting populations sampled at widely
349 different times in history, with divergence dates ranging from the Palaeolithic (up to ca.
350 87,000 yBP) to the "present" in the context of the dataset, and *randomly* splitting this graph
351 into "left" and "right" population sets.

352

353 ***Testing qpAdm performance on complex simulation histories***

354 Below we explore performance on simulated data (mainly FDR) of *qpAdm* protocols
355 representing the spectrum of protocols used in the literature. The most extreme example is
356 a protocol where all groups are rotated and all are treated alternatively as outgroups, targets,
357 and proxy sources, i.e., there is no temporal stratification between the latter categories. We
358 term this protocol “proximal rotating” (see Tables S1 and S2). Although such an extreme
359 situation is, to our knowledge, rare among published *qpAdm* protocols (see Calhoff et al.
360 2021, Oliveira et al. 2022; in the latter study the rotating *qpAdm* strategy was used to model
361 groups dated to 450–2600 yBP as mixtures of present-day groups), we use it to illustrate the
362 effects of poor temporal stratification of targets and proxy sources in the case of a rotating
363 protocol (Fig. 2). Models with targets pre-dating proxy sources are encountered in high-
364 throughput *qpAdm* screens, but do not constitute a majority of models (Narasimhan et al.
365 2019, Librado et al. 2021, Allentoft et al. 2022, Bergström et al. 2022, Lazaridis et al. 2022,
366 Taylor et al. 2023). We also explore FDR of the proximal non-rotating (Harney et al. 2018, van
367 de Loosdrecht et al. 2018, Narasimhan et al. 2019, Prendergast et al. 2019, Wang et al. 2020,
368 Calhoff et al. 2021, Wang et al. 2021, Zhang et al. 2021, Changmai et al. 2022a, Changmai et
369 al. 2022b, Maróti et al. 2022, Brielle et al. 2023, Lee et al. 2023), distal rotating (Narasimhan
370 et al. 2019, Librado et al. 2021, Allentoft et al. 2022, Bergström et al. 2022, Lazaridis et al.
371 2022, Taylor et al. 2023), and distal non-rotating protocols (Haak et al. 2015, Mathieson et al.
372 2015, Lazaridis et al. 2016, Antonio et al. 2019, Mathieson et al. 2018, Marcus et al. 2020,
373 Yang et al. 2020, Papac et al. 2021, Yaka et al. 2021, Patterson et al. 2022) (Tables 1 and 2).

374 In the distal protocols, only *qpAdm* models where target group's sampling date is strictly
375 contemporaneous with or post-dates sampling of both proxy sources were considered.

376 We tested performance of these *qpAdm* protocols on complex simulated genetic histories:
377 13 populations connected with each other by admixture graphs of random topology,
378 including 10 pulse-like admixture events. Ten diploid individuals with no missing data were
379 sampled from each population at "leaves" of the graph. Forty such random topologies were
380 simulated, with an upper bound on the graph depth at 800 generations (ca. 23,000 years in
381 the case of humans). These simulations generated sets of populations sampled at widely
382 different dates in the past or, in other words, located at various genetic distances from the
383 root, and matching intra-continental levels of human genetic differentiation (Fig. S1). Further
384 details on the simulated population histories are presented in Methods and illustrated by five
385 examples in Fig. S2. To explore the influence of data amount on *qpAdm* performance and
386 compare it across protocols, we generated two independent sets of ten simulation replicates
387 for each graph topology: with genomes composed of three or ten 100-Mbp-sized
388 chromosomes (see Fig. S3 for the number of SNP loci polymorphic in the simulated datasets).
389 These sets of simulations are referred to as "setup no. 1" and "setup no. 2" below. To explore
390 the parameter space further, we generated single simulation replicates for two further
391 setups: "setup no. 3", with maximal simulated history depth increased to 3,000 generations
392 (ca. 87,000 yBP for humans), scaling all dates up proportionally; and "setup no. 4", with all
393 terminal branches extended to the "present" of the simulation and sampled at that point.
394 These latter simulations generated populations with median F_{ST} at the inter-continental level
395 (no. 3) or below it (no. 4, Fig. S1).

396 A typical archaeogenetic dataset is composed of pseudo-haploid data with high proportions
397 of missing sites and with widely different group sizes, including singleton groups. To generate
398 more realistic "noisy" data, we also performed randomised subsampling of SNP datasets for
399 simulation setups no. 1 and 2 (300- and 1,000-Mbp-sized genomes), for one simulation
400 replicate per each setup (see Methods for details). The resulting data were pseudo-haploid,
401 had missing data rates ranging from 5% to 95% across individuals, and had uneven group sizes
402 ranging from 1 to 10 individuals. Ten independent subsampled datasets were generated for
403 each simulated topology (400 replicates in total per simulation setup), including in the case
404 of 300-Mbp-sized genomes from ca. 20,200 to 518,000 SNP loci with no missing data at the

group level and polymorphic across 13 groups (median = 89,700), and in the case of 1,000-Mbp-sized genomes from ca. 66,600 to 2,095,700 such SNPs (median = 259,400, Fig. S3).

As detailed in the preceding section, various versions of *qpAdm* protocols form a core of many recent archaeogenetic studies. These protocols are aimed at finding the simplest feasible *qpAdm* models for target groups, where feasibility is defined by setting a threshold for *qpAdm/qpWave* *p*-values and by setting plausibility criteria for admixture proportions estimated with *qpAdm*. Finding a feasible two-way or more complex admixture model for a target is often interpreted as solid evidence for gene flow, especially if the PCA and *ADMIXTURE* methods confirm the same signal. Thus, *qpAdm* protocols are used in fact as formal tests for admixture, whereas the latter two methods are not formal tests.

simulated toplogy no. 34:	polymorphic SNPs with no missing data	target	proxy source 1	proxy source 2	proxy source 1, inferred admixture proportion	proxy source 2, inferred admixture proportion	standard error of the admixture proportions	*qpAdm* *p*-value	*p*-value for 1-way model T=S1	*p*-value for 1-way model T=S2	*p*-value for 1-way model S1=S2	*f3*(T; S1, S2), Z-score
sampling date variable, 1,000 Mbp	1,796,083	H	A	C	63.8%	36.2%	1.4%	4.4E-26	1.8E-142	0.0E+00	0.0E+00	15.5
sampling date variable, 300 Mbp	539,274	H	A	C	62.4%	37.6%	2.3%	6.4E-06	9.8E-49	5.8E-125	0.0E+00	8.9
sampling date variable, deep divergence, 300 Mbp	1,032,128	H	A	C	60.1%	39.9%	1.1%	2.0E-62	6.3E-239	0.0E+00	0.0E+00	18.8
sampled at "present", 300 Mbp	768,376	H	A	C	68.0%	32.0%	3.2%	1.5E-02	9.6E-23	1.8E-66	1.3E-116	30.5
sampling date variable, 1,000 Mbp	1,796,083	H	A	G	57.4%	42.6%	1.6%	3.1E-18	1.8E-142	1.2E-228	0.0E+00	15.2
sampling date variable, 300 Mbp	539,274	H	A	G	60.6%	39.4%	2.5%	2.7E-05	9.8E-49	9.1E-112	3.2E-304	9.5
sampling date variable, deep divergence, 300 Mbp	1,032,128	H	A	G	53.6%	46.4%	1.7%	6.2E-34	6.3E-239	5.2E-279	0.0E+00	18.2
sampled at "present", 300 Mbp	768,376	H	A	G	61.0%	39.0%	3.1%	4.8E-01	9.6E-23	4.2E-88	3.4E-183	32.9

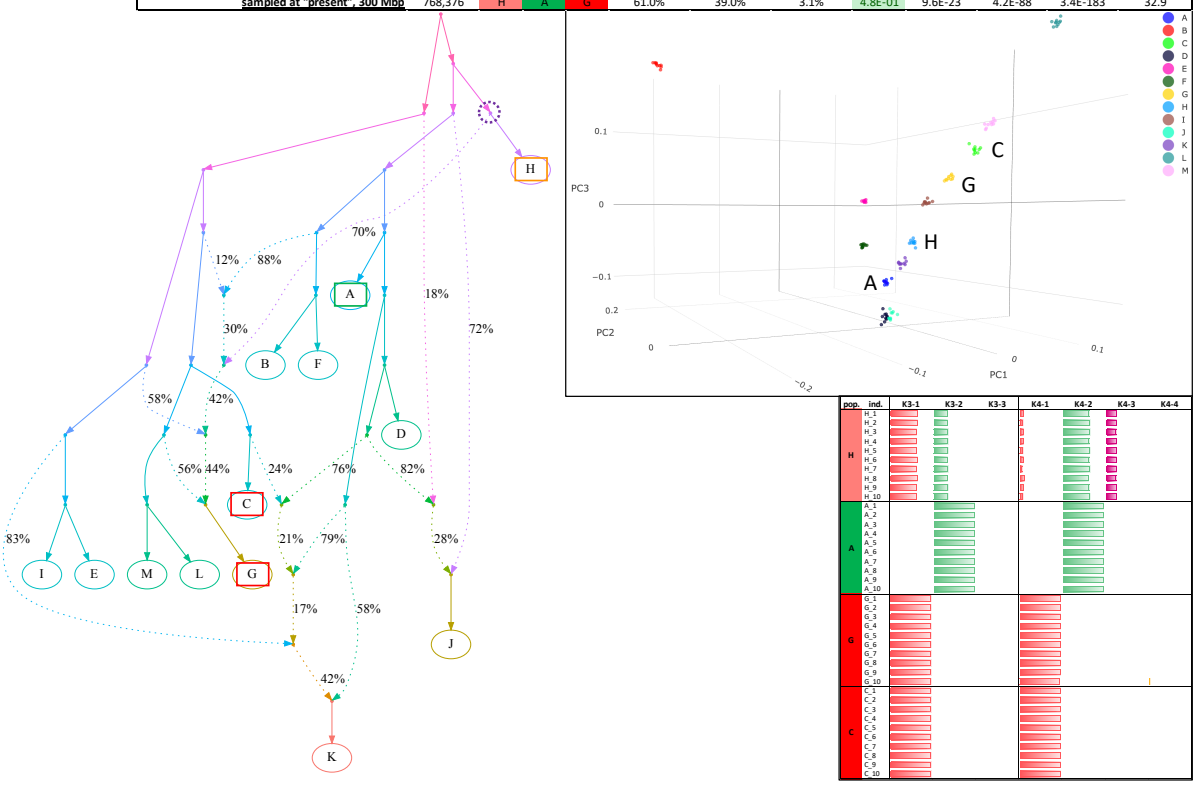

Figure 3. An example of the most common class of false positive *qpAdm* models supported by the proximal rotating protocol (accounts for 50.9% of all FP models across all the simulation and subsampling replicates in Table 2). Models of this type include at least one proxy ancestry source that is simulated as fully cladal with the target. The other proxy source may be simulated as a descendant

of the target lineage (see the model "*H = A + G*"), may belong to an unrelated lineage, or may be also cladal with the target (see the model "*H = A + C*"). Both models shown here are also fully supported by three-dimensional PCA and by an unsupervised *ADMIXTURE* analysis at one or more *K* values (under the simulation setup selected). For each model, the following information is shown: 1) simulation setups; 2) the number of polymorphic sites with no missing data at the group level; 3) admixture proportions and their standard errors estimated with *qpAdm*; 4) *p*-value of the two-way model; 5) *p*-values of the corresponding one-way models; 5) Z-score of the f_3-statistic f_3(target; proxy source$_1$, proxy source$_2$); 6) simulated admixture graph illustrating topological relationships among populations that are crucial for interpreting the models as false or true, but not dates of demographic events, sampling dates, and effective population sizes; 7) projection of a three-dimensional PCA plot with key groups labelled; 8) ancestry proportions estimated with unsupervised *ADMIXTURE* for the groups constituting the *qpAdm* models (results are shown for two selected *K* values). Items 6 to 8 are shown for the simulation setup whose name is underlined. Target groups are highlighted in orange throughout the figure; correct proxy sources are labelled in green, and incorrect ones in red. The true ancestry source for the target is marked by a dotted circle. The same selected (underlined) simulated history with dates, effective population sizes, and pairwise F_{ST} values is presented in Fig. S2a. For each simulation setup, results are shown for simulation replicate no. 1 only.

Relying on general principles, we argue that any high-throughput *qpAdm* protocol on poorly understood complex demographic relationships is questionable as a formal test for admixture since the *p*-value threshold allows to *reject*, but not to *accept* models, and it is safer to interpret those models as a certain number of gene flows connecting "left" and "right" sets in any direction, not in the form of proxy sources and admixture proportions for a target. The model feasibility criterion including both *p*-values and admixture proportions estimated with *qpAdm* is a complex construct relying on the topological assumptions outlined in Fig. 1. We expect that taking "left" and "right" sets that are not well-separated in time or contemporaneous (Fig. 2), and where relationships among groups are poorly understood (which is almost always true for exploratory studies), enriches the system for "left-to-right" gene flows, which in turn leads to frequent rejection of true simple admixture models. Since the behaviour of *qpAdm* admixture proportion estimates under different demographic scenarios is poorly understood, it is possible that a large fraction of these non-rejected complex models emerges as feasible, resulting in false signals of admixture.

The *qpAdm* protocols we applied to the simulated data were focused on the simplest models: one- and two-way admixture models (we note that histories that are more complex than two-way mixtures were common in the data, Fig. S2). The model feasibility criterion followed Narasimhan *et al*. (2019), see Box 1 for a definition. Thus, we tested all possible two-way

456 admixture models for 40 complex population histories (34,320 models per simulation setup
457 and replicate).

458 The non-rotating *qpAdm* approach was implemented as follows: for each simulated graph six
459 most ancient groups were selected as a fixed "right" set (ties were resolved in alphabetical
460 order; these "right" sets remained unchanged for a given graph topology across independent
461 simulations) and for the remaining seven groups all possible one-way and two-way admixture
462 models were tested, applying the same composite feasibility criterion that was used for the
463 rotating protocol.

464 In the context of complex and random admixture graph topologies it is hard to draw a strict
465 boundary between true and false admixture models composed of a target and only two proxy
466 sources. However, we classified the feasible *qpAdm* models into false and true ones relying
467 on a set of rules. By far the most common class of false feasible *qpAdm* models (referred to
468 as "false positive" or FP models), comprising 50.9% of all FP models generated by the
469 proximal rotating protocol across all the simulation and subsampling replicates (setups no. 1
470 and 2), occurs when the target group is rejected as forming a clade with one or both proxy
471 sources whilst they are simulated on graph topologies as clades. Interestingly, false cladality
472 rejection accounted only for 10.1% of FP models generated by the proximal non-rotating
473 protocol across all the simulation and subsampling replicates.

474 An example of this situation is shown in Fig. 3 where the clade relationship between the
475 target (*H*) and source (*A*) is rejected due "left-to-right" gene flows violating the topological
476 assumptions of *qpAdm*, and more complex models ("*H = A + C*" and "*H = A + G*") are evaluated
477 as true. When a true one-way model "*H = A*" is tested, *A* represents a proxy for the only true
478 source of ancestry in *H*, and outgroups *B*, *D*, and *F* split off the proxy branch after its
479 divergence from the true source (this situation is shown in Fig. 1e), and ancestry in outgroups
480 *J* and *K* is largely derived from that branch too (Fig. 1c), resulting in rejection of the one-way
481 model with a very low *p*-value, ~10^{-23} (Fig. 3). Removal of all these outgroups (*B, D, F, J, K*)
482 increases the *p*-value of the "*H = A*" model by many orders of magnitude, to 0.4. Models "*H*
483 *= B/C/D/F*" are also rejected with *p*-values below ~10^{-34}. Interestingly, not only the one-way
484 models, but all two-way models "*H = A/B/C/D/F + X*" were rejected according to *p*-values
485 under at least three of four simulation setups (Fig. 3; removal of certain outgroups was not

486 done). The FP models shown in Fig. 3 under simulation setup no. 4 cannot be filtered out by
487 temporal stratification of targets and sources since all groups were sampled at "present".

488 Other topological classes of FP models can be concisely described as follows (and are more
489 precisely defined in Methods): 1) a proxy source included in the model is symmetrically
490 related to all real sources of ancestry in the target (see an example of such feasible *qpAdm*
491 models in Fig. S4a), or both proxy sources represent the same true source and are
492 symmetrically related to all the other true sources (Fig. S4b); 2) both proxy sources represent
493 distinct real sources, however a proxy source is a heavily admixed group sharing less than
494 40% of ancestry with the real source (Fig. S4c); 3) gene flow goes from the target lineage
495 (after the last admixture event in its history) to the proxy source lineage, not in the opposite
496 direction (Fig. S4d). Two-way admixture models for targets with population history best
497 approximated with three-way and more complex models were considered as true positives if
498 they included source proxies *not* satisfying the false positivity criteria listed above for at least
499 two true sources. We also note that the class of models classified as true positive (TP) was
500 not restricted to those including most optimal source proxies, if the models do *not* satisfy the
501 false positivity criteria. On a random sample of 400 two-way admixture models from our 40
502 simulated histories, the fraction of models that were classified as appropriate (true)
503 according to the rules described above was 17.7%. Since groups that are truly admixed are
504 common in our simulations, we do not expect to encounter a "needle in a haystack" situation
505 where finding true admixture models is exceedingly hard.

506 Violations of the topological assumptions of *qpAdm* encountered in the examples of FP model
507 classes are described below. All the models shown below were selected among feasible
508 models that were outcomes of the proximal rotating protocol, and, for simplicity, *qpAdm*,
509 PCA, and *ADMIXTURE* results are presented for one simulation replicate per simulation setup.
510 In Fig. S4a, the target group, *A*, was simulated as a two-way mixture, and we expect that
511 models "*A = B + C/K*" would be fitting. The topological assumptions are violated when testing
512 these models (Fig. S4a): groups *C* and *K* are cladal, with one of them appearing in the "left"
513 set and the other one in the "right" set (see Fig. 1e); a gene flow from an outgroup branch,
514 *D*, enters the *C/K* branch after it splits from one of the true ancestry sources (Fig. 1a).
515 However, *p*-values of the models "*A = B + C/K*" are high (0.93, 0.97), and they were rejected
516 due to estimated admixture proportions being negative. Removal of the outgroups *C, D,* and

517 *K* does not make these models fitting. In contrast, incorrect models "*A = B + G/J*" emerged as
518 fitting (Fig. S4a), where the proxy sources *G* and *J* are symmetrically related to both true
519 ancestry sources in the target.

520 In Fig. S4b, the target group, *A*, was simulated as a two-way mixture, and both correct (*A = F*
521 *+ B*) and incorrect (*A = F + M*) models are fitting, suggesting that violations of the topological
522 assumptions play no role in the emergence of this false positive model. Failure to reject the
523 model "*A = F + M*", where both proxy sources represent only one true ancestry source and
524 are symmetrically related to the other, may be attributed to the lack of data, however
525 increasing the simulated genome size from 300 Mbp to 1,000 Mbp or increasing the
526 simulated graph depth from 800 to 3,000 generations resulted in rejections of both the
527 correct and incorrect models with *p*-values below ~10^{-5} (Fig. S4b).

528 In Fig. S4c, the target group, *E*, was simulated as a two-way mixture, but no appropriate
529 source proxy was simulated for one of the true ancestry sources: in groups *H* and *A*, 30% and
530 6% of their ancestry, respectively, is derived from that true source. Thus, multiple gene flows
531 from the "right" set enter the *A* lineage after its split from the true ancestry source, and the
532 same is true for the *H* lineage, and these are violations of the topological assumptions (Fig.
533 1a). The model "*E = H + L*" was rejected according to *p*-values under all four simulation setups,
534 and the model "*E = A + L*" was rejected according to *p*-values when more data was available
535 (the simulated genome size increased from 300 Mbp to 1,000 Mbp, or the simulated graph
536 depth increased from 800 to 3,000 generations, see Fig. S4c). Accepting models like "*E = A +*
537 *L*" at face value may lead to erroneous historical interpretations, but all thresholds for
538 classifying models of this type into false and true are arbitrary. We chose 40% as a threshold
539 percentage of proxy source's ancestry derived from the corresponding true source.

540 In Fig. S4d, the target group, *G*, was simulated as a two-way mixture, and an incorrect model
541 "*G = C + J*" emerged as fitting. Here, *J* is a descendant of *G* (87% of its ancestry) rather than a
542 proxy source (only ~2% of its ancestry is derived from one of the true ancestry sources). The
543 model "*G = C + J*" was rejected according to *p*-values when more data was available (the
544 simulated genome size increased from 300 Mbp to 1,000 Mbp, or the simulated graph depth
545 increased from 800 to 3,000 generations, see Fig. S4d). Correct models such as "*G = A + J*"
546 were rejected according to *p*-values (Fig. S4d) due to violations of the topological

547 assumptions: for instance, outgroups *C* and *I* are derived from the target lineage after the
548 admixture event (Fig. 1d). However, removal of various violating outgroups did not make the
549 model "*G = A + J*" and similar models "*G = L/M + J*" fitting.

550 While FP *qpAdm* models are expected for complex genetic histories, the practical usage of
551 the *qpAdm* relies on an assumption that false positives are rare. However, FDR of the four
552 *qpAdm* protocols tested here (rotating and non-rotating, proximal and distal) varied between
553 12.1% and 68.1% (across all simulation setups and replicates summarized in Table 1). Key
554 statistics in our study are false discovery rate (FDR) and false omission rate (FOR); see Box 1
555 for definitions. We estimated FDR and FOR instead of false positive and false negative rates
556 of the *qpAdm* protocols and other methods due to a technical limitation: the process of model
557 classification into true and false ones cannot be fully automated since it requires careful
558 interpretation of the topology and simulated admixture proportions. Therefore, classifying
559 all possible 34,320 two-way admixture models (858 per simulated topology) into true and
560 false was hardly feasible. We estimated false positive (FPR) and true positive rates (TPR) only
561 approximately, relying on the fractions of negatives and positives in random samples of two-
562 way admixture models (see below). FPR in our context is the probability that a two-way model
563 with an unadmixed target and/or inappropriate proxy source(s) emerges as fitting in a single
564 *qpAdm* test. TPR in our context is the probability that a two-way model with an admixed
565 target and both proxy sources being appropriate emerges as fitting in a *qpAdm* test.

566

567 ***Influence of the amount of data and temporal stratification on the performance of qpAdm***
568 ***protocols***

569 The amount of data (3.3-fold difference in simulated genome sizes) had no influence on FDR
570 of *qpAdm* protocols in the case of randomly subsampled pseudo-haploid data (no statistically
571 significant difference was found between sets of 10 subsampling replicates in the case of four
572 *qpAdm* protocols, Table 2, Fig. 4). In contrast, small but statistically significant influence of
573 the data amount on FDR (according to the two-sided Wilcoxon test) was observed for three
574 of four *qpAdm* protocols applied to high-quality data: proximal rotating and non-rotating, and
575 distal non-rotating (Table 2, Fig. 4).

simulation scheme	max. depth of the simulation, gen.	pseudohaploid noisy data	genome size, Mbp	model class	protocol	number of two-way models in the respective class (min.-max.)	fraction of models that are distal	min.-max. across 10 replicates	FDR for proximal & distal models	min.-max. across 10 replicates	FDR for distal models	min.-max. across 10 replicates	number of two-way models in the respective class	fraction of models that are distal	FDR for proximal & distal models	FDR for distal models	number of two-way models in the respective class	fraction of models that are distal	FDR for proximal & distal models	FDR for distal models
													supported by 3D PCA				supported by unsupervised *ADMIXTURE*			
date variable, no. 1 (noisy)	800	yes	300	FP	non-rotating	75 (62-95)	37.3%	30.6%-42.9%	37.4%	29.5%-42.3%	24.2%	17.6%-28.1%								
					rotating	642 (579-733)	20.9%	17.8%-24.6%	53.0%	51.6%-54.9%	25.1%	22.4%-29.0%								
				TP	non-rotating	146 (115-149)	67.0%	60.0%-76.4%												
					rotating	554 (492-613)	68.6%	66.7%-73.8%												
date variable, no. 2 (noisy)	800	yes	1000	FP	non-rotating	86 (76-102)	36.2%	28.2%-47.3%	39.3%	34.1%-41.2%	25.1%	18.6%-32.6%								
					rotating	417 (355-500)	19.4%	17.7%-23.5%	54.6%	51.7%-59.7%	24.0%	21.8%-27.9%								
				TP	non-rotating	133 (126-164)	66.8%	62.7%-72.5%												
					rotating	340 (297-405)	74.0%	70.1%-81.3%												
date variable, no. 1	800	no	300	FP	non-rotating	76 (62-92)	39.2%	34.5%-48.0%	42.6%	35.8%-45.5%	31.2%	24.5%-34.4%	20	30.0%	35.1%	18.2%	2	100.0%	4.5%	6.1%
													72	40.3%			90	36.7%		
					rotating	247 (194-268)	16.4%	10.5%-19.1%	57.4%	55.6%-62.6%	22.1%	14.4%-27.9%	129	7.8%	61.4%	14.3%	59	3.4%	49.6%	4.4%
													83	36.1%			153	24.8%		
				TP	non-rotating	105 (93-115)	65.5%	59.5%-71.2%					37	73.0%			42	73.8%		
													72	59.7%			67	58.2%		
					rotating	165 (149-202)	80.8%	78.1%-84.1%					81	74.1%			60	71.7%		
													92	89.1%			113	87.6%		
date variable, no.2	800	no	1000	FP	non-rotating	43 (32-62)	40.4%	26.8%-53.1%	38.4%	31.3%-41.5%	26.5%	16.4%-30.4%	14	35.7%	40.0%	23.8%	1	0.0%	3.2%	0.0%
													18	66.7%			31	54.8%		
					rotating	127 (106-139)	10.5%	6.0%-16.7%	62.0%	57.6%-68.1%	16.4%	12.1%-26.7%	84	3.6%	70.6%	10.3%	18	0.0%	40.9%	0.0%
													30	26.7%			96	11.5%		
				TP	non-rotating	75 (65-95)	66.0%	58.9%-74.7%					21	76.2%			30	80.0%		
													49	73.5%			40	70.0%		
					rotating	75 (65-84)	83.6%	80.0%-88.1%					35	74.3%			26	69.2%		
													49	91.8%			58	91.4%		
date variable, no. 3	3000	no	300	FP	non-rotating	36	38.9%		36.0%		24.1%		12	33.3%	34.3%	20.0%	5	20.0%	12.8%	5.3%
													24	41.7%			31	41.9%		
					rotating	61	16.4%		66.3%		25.6%		41	7.3%	77.4%	23.1%	12	8.3%	46.2%	7.7%
													20	35.0%			49	18.4%		
				TP	non-rotating	64	68.8%						23	69.6%			34	52.9%		
													41	68.3%			30	86.7%		
					rotating	31	93.5%						12	83.3%			14	85.7%		
													19	100.0%			17	100.0%		
at "present", no. 4	800	no	300	FP	non-rotating	99	40.4%		42.1%		30.3%		53	64.2%	36.1%	34.0%	18	72.2%	20.5%	19.1%
													46	13.0%			81	33.3%		
					rotating	364	17.6%		64.0%		29.8%		178	22.5%	59.5%	29.9%	59	22.0%	37.8%	15.1%
													186	12.9%			305	16.7%		
				TP	non-rotating	136	67.6%						94	70.2%			70	78.6%		
													42	61.9%			66	56.1%		
					rotating	205	73.7%						121	77.7%			97	75.3%		
													84	67.9%			108	72.2%		

Table 1. Assessing the effect of temporal stratification of targets and proxy sources on FDR of non-rotating and rotating *qpAdm* protocols and their combinations with PCA and *ADMIXTURE* analyses**.** Another kind of temporal stratification, stratification of the "right" and "left" sets, was a part of the non-rotating protocols, but not of the rotating ones. FDR values are highlighted in the respective columns and color-coded. In the right half of the table these FP and TP classes are further subdivided into those supported/not supported (highlighted in green and red, respectively) by another method (PCA or *ADMIXTURE*). For each model class and sub-class, fractions of models in the FP and TP classes that are distal are shown with magenta bars. If all groups were sampled at present (simulation setup no. 4), selection of time-stratified admixture models was performed as if they were sampled in the past (as in simulation setups no. 1-3) since simulated topologies were the same across all the setups and differed only in the amount of genetic drift on graph edges. In the case of simulation setups no. 1 and 2, 10 simulation replicates and 10 subsampling replicates derived from simulation replicate no. 1 were generated, and median, minimal, and maximal values across the replicates are shown for counts of FP and TP *qpAdm* models, for fractions of models that are distal, and for FDR.

592 In the case of the most extreme *qpAdm* protocol, proximal rotating, adding data increased
593 median FDR from 57.4% to 62%, and this difference is statistically significant (Table 2). A large
594 fraction of false positives in the case of the proximal rotating protocol emerges due to false
595 rejections of one-way models because of violations of the topological assumptions (Fig. 1),
596 for instance, due to "left-to-right" gene flows, and that prompts the investigator to test more
597 complex two-way models, which often emerge as feasible. And model rejection is more
598 efficient when more data are available, explaining the effect on FDR observed here. As we
599 show in Suppl. text 1, it is probably impossible to decrease FDR of the proximal rotating
600 protocol dramatically by combining it with other methods (PCA and unsupervised
601 *ADMIXTURE*) as additional controls or by adjusting *p*-value thresholds in the *qpAdm* protocol.

two-sided Wilcoxon test, *p*-value (paired test if *qpAdm* protocols differ, but simulation parameters are the same)									
max. depth of the simulation: 800 gen.		proximal rotating	proximal non-rotating	distal rotating	distal non-rotating	proximal rotating	proximal non-rotating	distal rotating	distal non-rotating
date variable sampling		300-Mbp-sized genomes				1000-Mbp-sized genomes			
subsampling replicates on pseudohaploid data									
proximal rotating	300 Mbp	53.0%	0.002	0.002	0.002	0.166			
proximal non-rotating	300 Mbp		37.4%	0.002	0.002		0.190		
distal rotating	300 Mbp			25.1%	0.160			0.579	
distal non-rotating	300 Mbp				24.2%				0.186
proximal rotating	1000 Mbp					54.6%	0.002	0.002	0.002
proximal non-rotating	1000 Mbp						39.3%	0.002	0.002
distal rotating	1000 Mbp							24.0%	0.625
distal non-rotating	1000 Mbp								25.1%
simulation replicates on high-quality data									
proximal rotating	300 Mbp	57.4%	0.002	0.002	0.002	0.009			
proximal non-rotating	300 Mbp		42.6%	0.002	0.002		0.009		
distal rotating	300 Mbp			22.1%	0.010			0.143	
distal non-rotating	300 Mbp				31.2%				0.003
proximal rotating	1000 Mbp					62.0%	0.002	0.002	0.002
proximal non-rotating	1000 Mbp						38.4%	0.002	0.002
distal rotating	1000 Mbp							16.4%	0.002
distal non-rotating	1000 Mbp								26.5%

602

603 **Table 2.** Comparing FDR of four *qpAdm* protocols, proximal and distal, rotating and non-rotating, on
604 10 subsampling replicates derived from a single simulation replicate (low-quality data) or on 10
605 simulation replicates and high-quality genomes (300-Mbp-sized or 1000-Mbp-sized genomes). For
606 details on generating replicates of low-quality data see Methods. Median FDR values for *qpAdm*
607 protocols are shown on the diagonal. The protocols were compared using the two-sided Wilcoxon
608 test applied to FDR values, see the cells above the diagonal.

609

610 However, in the case of both proximal and distal non-rotating protocols, adding data led to a
611 small but statistically significant decrease in FDR: 42.6% vs. 38.4%, 31.2% vs. 26.5% (Table 2,

612 Fig. 4), suggesting that false model rejections due to assumption violations play a less
613 important role here, which is expected for "right" and "left" population sets which are
614 stratified temporally. We found no significant effect of the data amount on FDR in the case
615 of the distal rotating protocol, which demonstrated the best median FDR values on high-
616 quality data overall (22.1 and 16.4%, Table 2, Fig. 4). We did not compare FDR between high-
617 quality and low-quality datasets with the Wilcoxon test since replicates in these cases were
618 generated differently (in the latter case subsampling replicates were derived from one
619 simulation replicate per simulation setup, while in the former case ten simulation replicates
620 were considered per simulation setup), but we note that random subsampling of SNPs and
621 individuals and a less robust algorithm for calculating f_4-statistics (with different statistics
622 calculated on different SNP sets) did not lead to dramatic increases/decreases in FDR (Table
623 2, Fig. 4).

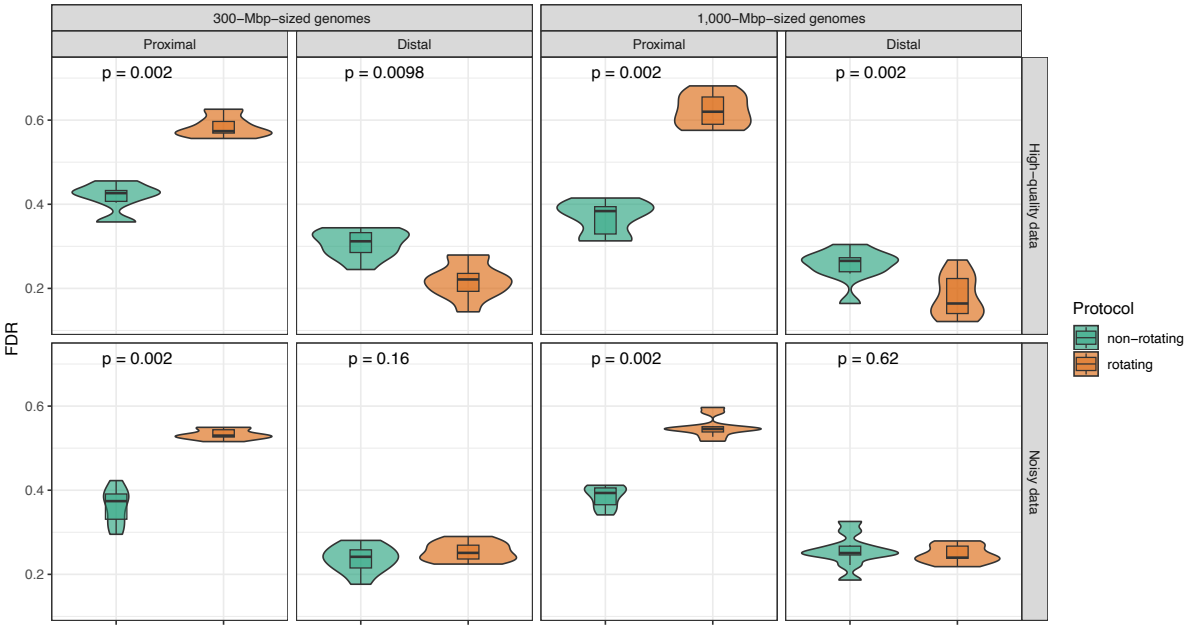

624

625 **Figure 4.** Distributions of FDR values across 10 simulation replicates (for high-quality data) or across
626 10 subsampling replicates derived from a single simulation replicate (for low-quality data).
627 Distributions are summarized with boxplots and violin plots for four *qpAdm* protocols (proximal and
628 distal, rotating and non-rotating) and two simulated genome sizes (300 Mbp and 1,000 Mbp). *qpAdm*
629 protocols were compared with the paired two-sided Wilcoxon test, and *p*-values for "rotating vs. non-
630 rotating" comparisons are shown in the panels (for the other *p*-values see Table 2).

631

632 Next, we move on to assessing the influence of *qpAdm* protocol details on FDR. Temporal
633 stratification of targets and proxy sources (the former are not allowed to pre-date the latter)
634 is the best way of reducing FDR, according to our analysis: from ~50%–60% to ~15%–25% for
635 rotating protocols, and from ~40% to ~25%–30% for non-rotating protocols (Table 2, Fig. 4).
636 All these differences are statistically significant according to the two-sided Wilcoxon test (the
637 paired version of the test was used in this case since different *qpAdm* protocols applied to
638 the same simulation/subsampling replicate are not totally independent experiments).
639 Temporal stratification of "right" and "left" sets (i.e., the non-rotating protocol) is helpful in
640 the absence of the former type of temporal stratification, of targets and proxy sources: FDR
641 drops from ~50%–60% to ~40% (these differences are also statistically significant, Table 2,
642 Fig. 4). However, it is not helpful (no significant difference) or even damaging to *qpAdm*
643 performance (significantly worse) when applied to distal protocols (Table 2, Fig. 4). This result
644 supports the conclusion by Harney et al. (2021) that rotating *qpAdm* protocols should be
645 preferred to non-rotating ones. However, according to our analysis, this conclusion is
646 conditional on strictly enforced temporal stratification of targets and proxy sources since the
647 rotating protocol without such stratification ("proximal rotating") demonstrated by far the
648 worst performance.

649 Another observation is that absolute FDR values are high for all *qpAdm* protocols tested
650 (median FDR values below 16.4% were not observed), however these absolute values are
651 expected to depend on the complexity of simulated histories and on the amount of data
652 (Table 2), which also depends on the time depth of simulated histories (Fig. S3, see
653 Discussion).

654 The fraction of two-way admixture models that are inappropriate according to our
655 topological criteria (the fraction of negatives) in a random sample of 400 models from all
656 simulated graphs is 82.3%, which allows us to approximately estimate not only FDR (51.6%–
657 68.1%, see Table 1), but the FPR of the proximal rotating protocol = number of false positives
658 per simulation replicate / number of negatives per simulation replicate [858 models × 40
659 graphs × fraction of negatives] = 0.4%–2.6% across simulation parameter combinations and
660 replicates summarized in Table 2. The TPR of the proximal rotating protocol = number of true
661 positives per simulation replicate / number of positives per simulation replicate [858 models

× 40 graphs × (1 – fraction of negatives)] = 1.1%–10.1%. Here are the same statistics for the distal non-rotating protocol: the fraction of negatives in a random sample of 400 distal non-rotating models from all simulated graphs, 74.3%; total number of distal non-rotating two-way models across all graphs, 1804; FDR across simulation parameter combinations and replicates from Table 2, 16.4%–34.4%; FPR, 0.8%–3.2%; TPR, 9.7%–24.4%. Thus, although FPR of a single *qpAdm* test is low, due to the relatively high proportion of negatives among all models, the large number of models tested in high-throughput *qpAdm* screens, and the low TPR, FDR becomes high, compromising historical interpretation of such screens for admixture.

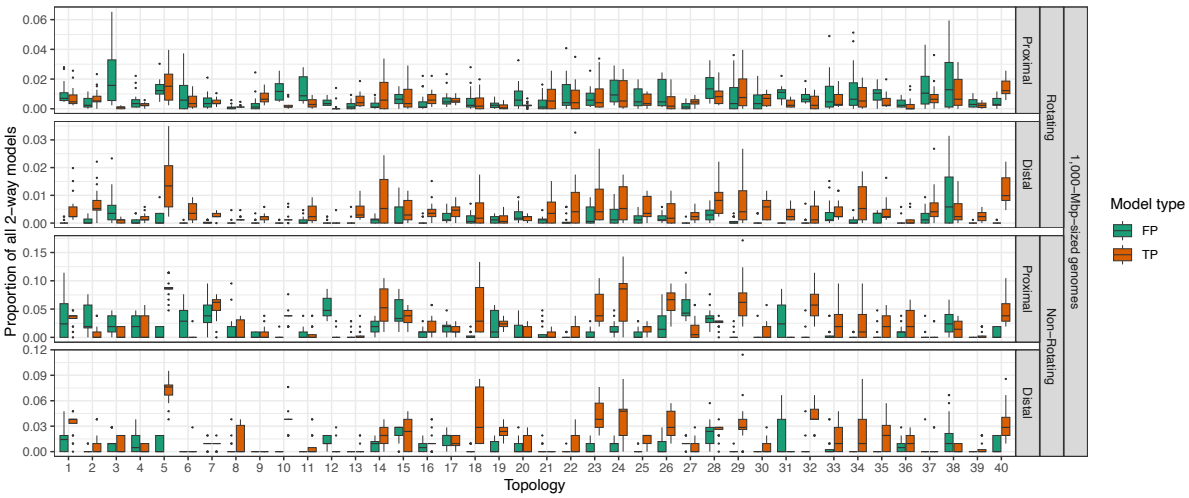

Figure 5. Proportions of all possible two-way *qpAdm* models that are false positive (FP), or true positive (TP), binned by simulated graph topology. There are 858 two-way admixture models per simulated graph including 13 groups if the rotating *qpAdm* protocol is applied, and 105 models if the non-rotating protocol is applied. For brevity, results are shown for simulation setup no. 2 (high-quality data) only. The boxplots summarize distributions of FP and TP model fractions across simulation replicates.

The fraction of feasible *qpAdm* models that are false (FP) varies a lot depending on simulated graph topology (Fig. 5), and hence it is hard to predict if a particular real genetic history is prone to generating FP signals of admixture when *qpAdm* protocols are applied. Among 80 combinations of proximal *qpAdm* protocols (rotating or non-rotating), simulation setups, and simulation/subsampling replicates we tested, in one case only a topology accounts for >20% of FP *qpAdm* models found across all the 40 simulated topologies. In contrast, in the case of distal *qpAdm* protocols, results are much more uneven across topologies: for 25 of 80

686 “protocol/simulation setup/replicate” combinations, at least one topology accounts for >20%
687 of FP *qpAdm* models found across all the 40 simulated topologies. Three topologies most
688 problematic for distal *qpAdm* protocols are illustrated in Fig. S5:

689

690 ***Admixture inference pipelines and model competition qpAdm protocols***

691 An implicit assumption of many archaeogenetic studies relying on *qpAdm* protocols is that
692 admixture models supported by clines observed in (usually two-dimensional) spaces of
693 principal components, and/or by an *ADMIXTURE* analysis, and/or by individual *D*-, f_4- or f_3-
694 statistics are especially robust. And, *vice versa*, *qpAdm* results are often interpreted as a
695 formal test of hypotheses about admixture formulated based on PCA and/or *ADMIXTURE*
696 results. We constructed “admixture inference pipelines” composed of a *qpAdm* protocol and
697 one or two further methods to test these assumptions on simulated data. We note that all
698 signals of admixture revealed by our PCA or *ADMIXTURE* analyses were not explored with
699 *qpAdm* since exhaustive lists of positive and negative two-way admixture models were not
700 compiled for each simulated graph. *Vice versa*, all feasible *qpAdm* models were checked by
701 the PCA and/or *ADMIXTURE* methods.

702 We considered a two-way admixture model to be supported by PCA if the target group was
703 located on a straight line between the two proxy source groups in the space of three PCs
704 when all 13 simulated groups were co-analysed. Deviation from the straight line was
705 acceptable to some extent as non-linear PCA clines are often observed on real data (de Barros
706 Damgaard et al. 2018, Jeong et al. 2019), and they were also common among TP two-way
707 *qpAdm* models in this study (see Methods for details and Figs. 3 and S4 for examples). This
708 situation is expected since many targets in our simulations represent three-way and more
709 complex mixtures, and since arrangement of populations in the PC space is influenced not
710 only by admixture, but also by genetic drift (McVean 2009). Our requirements for a model to
711 be declared supported by PCA were more stringent than those usually applied in the
712 literature since we considered three-dimensional PC spaces instead of two-dimensional ones.
713 Also see Methods for the rules we used to judge if an admixture model is supported by an
714 unsupervised *ADMIXTURE* analysis, and see Figs. 3 and S4 for examples.

715 A much more limited form of group rotation, “model competition”, is used in the literature
716 widely (Narasimhan et al. 2019, Fernandes et al. 2020, Calhoff et al. 2021, Sirak et al. 2021,
717 Zhang et al. 2021, Maróti et al. 2022, Brielle et al. 2023, Lee et al. 2023), and we explored FDR
718 of this method as well. A typical model competition protocol (Narasimhan et al. 2019, Maróti
719 et al. 2022, Brielle et al. 2023) consists of two stages. First, the oldest, e.g., Palaeolithic,
720 populations (and/or those most divergent from the target group) are used as a fixed “right”
721 set, and populations sampled at later dates are used as proxy sources and targets. As usual,
722 progressively more complex models are tested for targets of interest, and a composite
723 feasibility criterion is applied.

724 In many publications (e.g., Haak et al. 2015, Mathieson et al. 2015, Antonio et al. 2019,
725 Mathieson et al. 2018, Prendergast et al. 2019, Marcus et al. 2020, Papac et al. 2021, Wang
726 et al. 2021, Yaka et al. 2021, Changmai et al. 2022a, 2022b, Patterson et al. 2022) this first
727 non-rotating step remains the only *qpAdm* protocol used (in its distal or proximal forms). In
728 a model competition protocol, subsequent analysis is focused on targets for whom two or
729 more alternative *qpAdm* models emerge as feasible at the first step. For each target,
730 alternative proxy sources are pooled and rotated between the “left” and “right” sets, testing
731 only the models that emerged as feasible at the first step and applying a composite feasibility
732 criterion (e.g., p-value > 0.01, estimated admixture proportions ± 2 SE are within 0 and 1).

733 Rotation of alternative proxy sources can be performed in various ways: “whatever is not on
734 the left is on the right” (Brielle et al. 2023), or placing alternative sources in the ”right” set
735 one by one (Calhoff et al. 2021, Maróti et al. 2022, Brielle et al. 2023). In the latter case several
736 “right” sets are tested for each model, and the model is considered supported by the model
737 competition protocol only if it is not rejected under any of these “right” sets (Maróti et al.
738 2022). The reasoning behind this protocol is as follows: model rejection due to violations of
739 the topological assumptions of *qpAdm* is not expected for a model composed of sources very
740 close to the true ones since in this case branches private to the proxy sources are short, and
741 it is unlikely that gene flows to or from the “right” set happened on these short branches.
742 Models composed of sources closely related to the true ones are also not expected to be
743 rejected when more distant proxy sources are placed in the “right” set (Harney et al. 2021).

For reasons detailed in the Discussion section, we explored the *qpAdm* model competition protocol and multi-method admixture inference pipelines on one replicate per simulation setup, and three (Table 3) or four (Table 1) simulation setups were involved in this analysis.

two-way models supported by:	simulation scheme	max. depth of the simulation, gen.	pseudohaploid noisy data	genome size, Mbp	feasible *qpAdm* models/ all 2-way models	non-rotating *qpAdm* with temporal stratification of the R and L sets, but with no stratification of targets and proxy sources				one or two alternative sources "on the left", all others "on the right"				one or two alternative sources "on the left", all others "on the right", one at a time			
proximal non-rotating *qpAdm*						1	1	1	1	1	1	1	1	1	1	1	1
qpAdm model competition										2	2	2	2	2	2	2	2
"admixture" *f3*- statistics							2										
3D PCA								2			3		3		3		3
unsupervised *ADMIXTURE*									2			3	4			3	4
	date variable, no. 1	800	no	300	201/ 4,200 (4.8%)	45.8%	0.0%	10.0%	1.0%	16.4%	6.0%	0.0%	0.0%	15.9%	5.0%	0.0%	0.0%
													6.0%				5.0%
											10.4%	16.4%	0.0%		10.9%	15.9%	0.0%
													10.4%				10.9%
							45.8%	35.8%	44.8%	29.4%	4.0%	1.0%	0.0%	29.9%	5.0%	1.0%	0.0%
													4.0%				5.0%
											25.4%	28.4%	1.0%		24.9%	28.9%	1.0%
													24.4%				23.9%
						54.2%	2.5%	18.4%	20.9%	19.4%	7.5%	10.0%	4.5%	22.4%	8.5%	10.4%	5.5%
													3.0%				3.0%
											11.9%	9.5%	5.5%		13.9%	11.9%	5.0%
													6.5%				9.0%
							51.7%	35.8%	33.3%	34.8%	10.9%	10.9%	4.0%	31.8%	10.0%	10.4%	3.0%
													7.0%				7.0%
											23.9%	23.9%	7.0%		21.9%	21.4%	7.5%
													16.9%				14.4%
					FDR	45.8%	0%	35.1%	4.5%	45.8%	44.4%	0%	0%	41.6%	37.0%	0%	0%
					FOR	0%	95.4%	66.1%	61.5%	64.2%	86.2%	81.7%	91.7%	58.7%	84.4%	80.7%	89.9%
	date variable, no. 3	3000	no	300	100/ 4,200 (2.4%)	36.0%	0.0%	12.0%	5.0%	8.0%	6.0%	2.0%	2.0%	8.0%	6.0%	2.0%	2.0%
													4.0%				4.0%
											2.0%	6.0%	0.0%		2.0%	6.0%	0.0%
													2.0%				2.0%
							36.0%	24.0%	31.0%	28.0%	6.0%	3.0%	3.0%	28.0%	6.0%	3.0%	3.0%
													3.0%				3.0%
											22.0%	25.0%	0.0%		22.0%	25.0%	0.0%
													22.0%				22.0%
						64.0%	4.0%	23.0%	34.0%	20.0%	5.0%	7.0%	4.0%	18.0%	5.0%	7.0%	4.0%
													1.0%				1.0%
											15.0%	13.0%	3.0%		13.0%	11.0%	3.0%
													12.0%				10.0%
							60.0%	41.0%	30.0%	44.0%	18.0%	27.0%	15.0%	46.0%	18.0%	27.0%	15.0%
													3.0%				3.0%
											26.0%	17.0%	12.0%		28.0%	19.0%	12.0%
													14.0%				16.0%
					FDR	36.0%	0%	34.3%	12.8%	28.6%	54.5%	22.2%	33.3%	30.8%	54.5%	22.2%	33.3%
					FOR	0%	93.8%	64.1%	46.9%	68.8%	92.2%	89.1%	93.8%	71.9%	92.2%	89.1%	93.8%
	at 'present', no. 4	800	no	300	235/ 4,200 (5.6%)	42.1%	0.0%	22.6%	7.7%	13.6%	9.4%	5.1%	3.8%	11.9%	7.7%	4.3%	3.0%
													5.5%				4.7%
											4.3%	8.5%	1.3%		4.3%	7.7%	1.3%
													3.0%				3.0%
							42.1%	19.6%	34.5%	28.5%	13.2%	2.6%	2.1%	30.2%	14.9%	3.4%	3.0%
													11.1%				11.9%
											15.3%	26.0%	0.4%		15.3%	26.8%	0.4%
													14.9%				14.9%
						57.9%	2.6%	40.0%	29.8%	22.1%	15.7%	11.9%	10.2%	23.8%	17.0%	13.2%	11.1%
													5.5%				6.0%
											6.4%	10.2%	1.7%		6.8%	10.6%	2.1%
													4.7%				4.7%
							55.3%	17.9%	28.1%	35.7%	24.3%	17.9%	14.5%	34.0%	23.0%	16.6%	13.6%
													9.8%				9.4%
											11.5%	17.9%	3.4%		11.1%	17.4%	3.0%
													8.1%				8.1%
					FDR	42.1%	0%	36.1%	20.5%	38.1%	37.3%	30.0%	27.3%	33.3%	31.0%	24.4%	21.2%
					FOR	0%	95.6%	30.9%	48.5%	61.8%	72.8%	79.4%	82.4%	58.8%	70.6%	77.2%	80.9%

Table 3. Assessing FDR of the proximal non-rotating *qpAdm* protocol combined with model competition (Narasimhan et al. 2019). For each simulation setup, the analysis relies on simulation replicate no. 1 only. For constructing pipelines resembling those common in the archaeogenetic literature, we used five methods: proximal non-rotating *qpAdm*, *qpAdm* model competition (two alternative protocols), "admixture" f_3-statistics, 3D PCA with all individuals co-analysed, and unsupervised *ADMIXTURE* with all individuals co-analysed. For declaring a positive result, support of an admixture model by all methods in the pipeline was required, hence the order of methods is not

important except for the first method, which was the proximal non-rotating *qpAdm* in all cases. In each column, methods comprising a pipeline are color-coded and numbered by their order. All feasible two-way *qpAdm* models emerging as outcomes of the proximal non-rotating protocol were classified into FP and TP (highlighted in red and green in the leftmost column, respectively). The other columns are structured like bifurcating trees: FP *qpAdm* models supported by method no. 2; FP *qpAdm* models not supported by method no. 2; TP *qpAdm* models supported by method no. 2; TP *qpAdm* models not supported by method no. 2. The same principle is used for representing results of more complex pipelines. All model counts are normalized by the number of feasible *qpAdm* models (FP + TP), outcomes of the first method. Percentages of models supported/not supported by the last method in the pipeline are highlighted in green and red, respectively. FDR values are shown for these different pipelines. Fractions of TP *qpAdm* models that are pruned out by progressively more stringent support requirements are also shown (false omission rate or FOR).

The two alternative model competition protocols described above were applied to targets for whom more than one model was feasible given a fixed "right" set. If only one model was feasible for a target, such a model was evaluated as passing model competition (such models accounted only for 7%–11% of models feasible at the first step). The model competition protocols failed to improve *qpAdm* performance: FDR ranged from 29% to 46% (as compared to 36%–46% prior to the model competition step), and both model competition protocols demonstrated very similar results (Table 3). FOR of the model competition protocols varied from 59% to 72%. FDR also remained high for models supported by proximal non-rotating *qpAdm* & PCA or by proximal non-rotating *qpAdm* & model competition & PCA (Table 3).

Considering all simulation setups and replicates shown in Table 2, there were only 1,591 instances when a two-way admixture model was supported by both the proximal rotating and proximal non-rotating protocols on the same simulated data. In contrast, there were 5,844 and 24,046 instances when a model was supported exclusively by the proximal non-rotating and rotating protocols, respectively. Notably, FP models supported by the proximal non-rotating *qpAdm* protocol largely lacked support by an unsupervised *ADMIXTURE* analysis (Table 3), in contrast to outcomes of the proximal rotating protocol (Table S1). FDR of a pipeline composed of these two methods ranged from 5% to 21% across three simulation setups tested (Table 3). Adding a model competition step to this pipeline increased both FDR and FOR in 4 of 6 cases; and, in general, the proximal non-rotating *qpAdm* protocol combined with *ADMIXTURE* is the best-performing protocol in this analysis (Table 3) according to FDR and FOR.

789 The fact that our *ADMIXTURE* analysis supports a large fraction of FP two-way mixture models
790 emerging as outcomes of the proximal rotating *qpAdm* protocol reflects known problems in
791 modelling using *ADMIXTURE* very ancient individuals in the context of modern populations.
792 These individuals are often modelled (Raghavan et al. 2014, Haak et al. 2015, Moreno-Mayar
793 et al. 2018a) as complex mixtures of ancestry components typical for modern populations,
794 which is obviously an artefact. Sampling dates for unique targets from FP models supported
795 by both proximal rotating *qpAdm* and *ADMIXTURE* ranged from the present to 665
796 generations in the past (median = 406 generations), while the median sampling date for
797 unique targets from both FP and TP models supported by proximal rotating *qpAdm* was 215
798 generations in the past (for comparison across simulation setups, all the dates were rescaled
799 to a maximum simulation depth of 800 generations). The proximal non-rotating protocol by
800 design did not consider the oldest groups as targets for *qpAdm* and *ADMIXTURE*, thus largely
801 avoiding this problem (sampling dates for unique targets from FP models supported by both
802 proximal non-rotating *qpAdm* and *ADMIXTURE* ranged from the present to 366 generations
803 in the past; median = 44 generations).

804 Above we have discussed multi-method pipelines based on the proximal non-rotating *qpAdm*
805 protocol. Combining distal *qpAdm* protocols with PCA allows to reduce FDR of both rotating
806 and non-rotating protocols further, to 10%–24%, and distal *qpAdm* protocols combined with
807 an unsupervised *ADMIXTURE* analysis demonstrated even better FDR values ca. 0%–8%
808 (Table 1). If target and proxy source populations are sampled at approximately the same time
809 (such as those from our simulation setup no. 4 and from the proximal analysis in Narasimhan
810 et al. 2019, Fig. 2c) applying this approach is impossible. However, if our simulations with all
811 branches extended to the present are treated in the same way as their topological
812 counterparts with date-variable sampling, performance gains (decrease in FDR) of temporal
813 stratification of admixture models are similar to those mentioned above (Table 1). In this case
814 the temporal stratification procedure retains models with the latest admixture event in
815 target's history that is more recent than (or as recent as) the latest admixture events in proxy
816 sources' history. However, in the case of simulation setup no. 4 performance gains of the
817 "*qpAdm* + PCA" and "*qpAdm* + *ADMIXTURE*" method combinations were moderate (Table 1).

818

Discussion

In this study we explored performance of various *qpAdm* protocols on a collection of random complex simulated genetic histories, where admixture history of target groups may vary from the simplest (no admixture) to very complex. It is because of this research design and other limitations discussed below that our study is focused mostly on one performance metric: false discovery rate or FDR. In simple terms, we focused our analysis only on models of a chosen complexity class (two-way models) supported by a *qpAdm* protocol (feasible models), classified them manually into false and true positives according to a set of topological rules, and subjected them to further screening by PCA and/or *ADMIXTURE* methods. We did not attempt to classify rejections of two-way models by *qpAdm* or other methods into false rejections due to violations of the topological assumptions of *qpAdm* (Fig. 1) and true rejections when the true admixture history of the target does not fit a two-way model. This problem was deliberately left out since in the literature more attention is paid to interpretation of “fitting” (“feasible” or “positive”) than rejected *qpAdm* models.

Another limitation of our study is that we had to use idealized versions of *qpAdm*, PCA, and *ADMIXTURE* protocols, while in the archaeogenetic literature manual adjustment of analytical protocols is common: protocols often vary from one target group to another (see, e.g., Lazaridis et al. 2016, Zhang et al. 2021, Brielle et al. 2023, Lee et al. 2023) and from study to study. These extensive details are very hard to formalize and reproduce. In the case of *qpAdm* protocols, certain groups of populations may be placed exclusively in the “right" or in the “left" sets, with the rest rotated between these sets, and relative sizes and compositions of these three groups vary from study to study: in the case of model competition protocols, this rotated subset is small, and rotation may be restricted to a particular model complexity class, but in other cases it may encompass all or nearly all populations analysed (see, e.g., Narasimhan et al. 2019, Librado et al. 2021, Bergström et al. 2022, Lazaridis et al. 2022, Oliveira et al. 2022, Taylor et al. 2023). Reproducing all aspects of PCA and *ADMIXTURE* protocols used in the literature is also hardly possible on simulated data. For instance, PCs in archaeogenetic studies are usually calculated based on present-day populations, and ancient individuals are projected on the resulting PCs (e.g., Haak et al. 2015, Mathieson et al. 2018, Narasimhan et al. 2019, Furtwängler et al. 2020, Marcus et al. 2020, Lazaridis et al. 2022). In

849 contrast, in our study all simulated individuals were co-analysed for calculating PCs.
850 *ADMIXTURE* analyses in the literature are usually performed on worldwide or continent-wide
851 panels of populations that often overlap just partially with population sets used for *qpAdm*
852 analyses (see, for instance, Rasmussen et al. 2010, Haak et al. 2015, Harney et al. 2018,
853 Moreno-Mayar et al. 2018a, Zhang et al. 2021, Changmai et al. 2022a, Brielle et al. 2023),
854 while in our study identical population sets were used for *qpAdm*, PCA, and *ADMIXTURE*
855 analyses.

856 Another important caveat is that complexity of genetic history in the region and period of
857 interest often remains unknown and it is difficult to judge if a particular admixture graph
858 complexity is adequate for simulating the real history. However, we have not explored *qpAdm*
859 performance over a range of simulated admixture graph complexities, over a range of model
860 feasibility criteria (except for those in Table S2), for models more complex than two-way, and
861 have estimated FDR and FOR instead of false positive and false negative rates due to an
862 important technical limitation: the process of model classification into true and false ones
863 cannot be fully automated since it requires careful interpretation of the simulated topology
864 and simulated admixture proportions. For similar reasons, some comparisons of method
865 performance in this study, such as *qpAdm* vs. "*qpAdm* combined with *ADMIXTURE*", are
866 qualitative rather than quantitative: we applied the PCA and *ADMIXTURE* methods to one
867 simulation replicate only per simulation setup since automated classifiers of admixture
868 models into positive and negative ones based on 3D PCA and *ADMIXTURE* results were not
869 available. Despite these limitations, our simulations reproduce the most important aspects
870 of typical *qpAdm* protocols.

871 We demonstrated that application of the proximal rotating *qpAdm* protocol that can be
872 summarized as "whatever is not on the right is on the left" without any temporal stratification
873 of the "right" and "left" sets and of proxy sources and targets carries a risk of an FDR above
874 50% or 60%. Adding further levels of support (considering only models supported by PCA
875 and/or an *ADMIXTURE* analysis) does not help to decrease FDR drastically in this case (Table
876 S1, Suppl. text 1).

877 The proximal rotating protocol is an extreme example of *qpAdm* protocols that is rarely
878 encountered in the archaeogenetic literature (Calhoff et al. 2021, Oliveira et al. 2022) but

879 serves as a reference point in our analysis. Other protocols such as distal rotating (e.g.,
880 Narasimhan et al. 2019, Librado et al. 2021, Allentoft et al. 2022, Bergström et al. 2022,
881 Lazaridis et al. 2022, Taylor et al. 2023), distal non-rotating (e.g., Haak et al. 2015, Mathieson
882 et al. 2015, Lazaridis et al. 2016, Antonio et al. 2019, Marcus et al. 2020, Yang et al. 2020,
883 Papac et al. 2021, Yaka et al. 2021, Patterson et al. 2022), and proximal model competition
884 (e.g., Narasimhan et al. 2019, Calhoff et al. 2021, Zhang et al. 2021, Maróti et al. 2022, Brielle
885 et al. 2023, Lee et al. 2023) are often used in practice, and FDR of these three classes of
886 protocols on our simulated data ranged from 12% to 46% across simulation parameter
887 combinations and replicates (Tables 1 and 3). These FDR for best-performing standalone
888 *qpAdm* protocols are high but should not be over-interpreted since they are expected to
889 depend on the complexity of simulated histories and on the amount of data (Table 2), which
890 also depends on the time depth of simulated histories (Fig. S3). Only one graph complexity
891 level was tested, that is 13 groups and 10 admixture events; and only one time depth, 800
892 generations, was tested in a high-throughput way (Table 1). Thus, it is hard to extrapolate this
893 aspect of our results to real analyses and predict FDR levels on real data.

894 Temporal stratification tested in this study and practiced in the literature is of two sorts: 1)
895 most or all populations in the "right" set are sampled deeper in the past than those in the
896 "left" set (non-rotating protocols); 2) a target group post-dates (or is as old as) all its proxy
897 sources (distal protocols). We showed that both temporal stratification approaches helped
898 to decrease FDR of *qpAdm* admixture screens significantly, and the latter approach
899 demonstrated the best FDR among standalone *qpAdm* protocols (Table 2).

900 Although restricting analyses to distal models is often *necessary* for reducing FDR below an
901 arbitrary threshold at 10%, it is not *sufficient* for reaching this objective (Table 1) given the
902 complexity of our simulated admixture graph-shaped histories and the amounts of data we
903 generated. Respecting this threshold, only the following admixture screening protocols
904 demonstrated acceptable performance (we did not consider protocols demonstrating FOR
905 above 90% as useful in practice):

906 1) proximal non-rotating *qpAdm* with a requirement that admixture models are supported by
907 both *qpAdm* and an unsupervised *ADMIXTURE* analysis (Tables 1 and 3), under simulation

908 setups no. 1 and 2 (groups sampled at different dates in the past, maximal simulated history
909 depth = 800 generations, 300-Mbp-sized or 1000-Mbp-sized genomes simulated);

910 2) distal non-rotating or rotating *qpAdm* with a requirement that admixture models are
911 supported by both *qpAdm* and an unsupervised *ADMIXTURE* analysis (Table 1), under
912 simulation setups no. 1, 2, and 3 (groups sampled at different dates in the past, maximal
913 simulated history depth = 800 or 3000 generations, 300-Mbp-sized or 1000-Mbp-sized
914 genomes simulated).

915 FDR of these protocols was 0% – 8% (Table 1). In contrast, adding a model competition step
916 to the proximal non-rotating *qpAdm* protocol did not help to reduce FDR below 10%. The
917 performance of this type of protocols is explored in detail in Table 3. To sum up, we make the
918 following suggestions for improving robustness of admixture inference in archaeogenetics:

919 1. Our results suggest that temporal stratification of targets and proxy sources is a very
920 efficient way of reducing FDR of *qpAdm* protocols (Tables 1 and 2, Fig. 4). The distal
921 rotating and non-rotating protocols invariably demonstrated FDR significantly lower than
922 those of the proximal non-rotating and rotating protocols (Table 2). Although the
923 proximal model competition protocol (Narasimhan et al. 2019, Calhoff et al. 2021, Zhang
924 et al. 2021, Maróti et al. 2022, Brielle et al. 2023, Lee et al. 2023) was not tested on
925 multiple simulation or subsampling replicates (Table 3, we note that it demonstrated FDR
926 values higher than those of the distal non-rotating protocol (Table 1). Our results imply
927 that *qpAdm* protocols where all populations are sampled at present (similar to our setup
928 no. 4; see also Jeong et al. 2019, Changmai et al. 2022a) or where present-day groups are
929 used as proxy ancestry sources for ancient groups (e.g., Mathieson et al. 2015, van de
930 Loosdrecht et al. 2018, Narasimhan et al. 2019, Prendergast et al. 2019, Shinde et al. 2019,
931 Wang et al. 2020, Wang et al. 2021, Changmai et al. 2022b, Calhoff et al. 2021, Oliveira et
932 al. 2022) are less reliable than those where target groups are not allowed to pre-date
933 their proxy sources. While the proximal non-rotating *qpAdm* protocol demonstrated FDR
934 significantly lower than that of the proximal rotating protocol (Table 2), the distal rotating
935 protocol was in terms of FDR as good as the distal non-rotating protocol (on low-quality
936 data) or significantly better (on high-quality data, Table 2).

937 2. Another way of radically improving FDR of *qpAdm* protocols is combining *qpAdm* with an
938 unsupervised *ADMIXTURE* analysis. These two approaches should probably be combined
939 for optimal performance (Table 1).
940 3. Adding 3.3 times more data led to a small but significant decrease in FDR only in the case
941 of high-quality diploid data, but not in the case of pseudo-haploid data with high missing
942 rates (Table 2). This observation deserves further investigation.
943 4. It is safest to use the *qpAdm* method in controlled conditions, when relationships among
944 populations are understood well enough to exclude violations of the topological
945 assumptions, when radiocarbon or context dates of ancient populations are reliable and
946 allow accurate temporal stratification, or when sets of potential proxy sources are well-
947 constrained based on archaeological or historical scholarship: see, for instance, the
948 earliest publications where the *qpAdm* method was employed (Haak et al. 2015,
949 Mathieson et al. 2015) and some recent studies (e.g., Marcus et al. 2020, Papac et al.
950 2021, Yaka et al. 2021, Changmai et al. 2022a, 2022b, Patterson et al. 2022). Obviously,
951 the amount of new information that the *qpAdm* method provides in these conditions is
952 limited. However, considering that it was possible to reach FDR levels as low as 0% to 8%
953 on our simulated data, we do not recommend avoiding *qpAdm*-based high-throughput
954 admixture screens altogether.
955 5. Summing up all the results above, for reducing FDR of *qpAdm* admixture screens to nearly
956 0% we suggest using large SNP sets with low missing data rates, using the rotating *qpAdm*
957 protocol with a strictly enforced rule that targets do not pre-date their proxy sources, and
958 performing an unsupervised *ADMIXTURE* analysis to verify feasible *qpAdm* models.
959 6. Our study has multiple limitations and caveats discussed above, mostly related to
960 difficulties in simulating all the details of published *qpAdm*, PCA, and *ADMIXTURE*
961 protocols, to uncertainties about the level of admixture graph complexity that is adequate
962 for simulating real population histories (all our simulations were of the same complexity:
963 13 groups and 10 pulse-like admixture events), to difficulties in interpreting topologies of
964 random admixture graphs in an automated way for classifying even simple admixture
965 models into true and false ones, and to difficulties in interpreting 3D PCA and *ADMIXTURE*
966 results in an automated way. Nevertheless, our results surpass in scale previous
967 simulation studies of *qpAdm* protocols (Lazaridis et al. 2017, Ning et al. 2020, Harney et

968 al. 2021) by several orders of magnitude and may serve as a guide for users of high-
969 throughput *qpAdm* protocols.

970 7. Feasible *qpAdm* models are sometimes ranked by *p*-values, with a model having the
971 highest *p*-value highlighted as the most plausible one (see, for instance, Lazaridis et al.
972 2022, van de Loosdrecht et al. 2018, Oliveira et al. 2022, Taylor et al. 2023). *qpWave p*-
973 values for pairs of individuals were also used in lieu of genetic distances in the former
974 study (Lazaridis et al. 2022). Of 1,201 instances when both false and true feasible *qpAdm*
975 models were found for the same target group on the same data (all simulation setups,
976 simulation/subsampling replicates, and *qpAdm* protocols), a model having the highest *p*-
977 value was an FP in 463 (38.6%) cases, and the difference in maximal *p*-values between the
978 TP and FP model classes was significant according to the paired two-sided Wilcoxon test
979 (TP > FP, *p*-value = 2.2×10^{-16}). Thus, our limited analysis suggests that the approach of
980 ranking *qpAdm* models by *p*-values is justified (see also related results in Fig. S6 and Table
981 S2), but it generates noisy results.

982 8. f_3-statistic is a simple method for proving that a population is admixed, and it
983 demonstrated FDR values much lower (6%, see Suppl. text 1) than those of standalone
984 *qpAdm* protocols, but f_3-statistics are applicable only to recent admixture events and/or
985 populations of large effective size since post-admixture drift on the target lineage
986 obscures the signal. Moreover, calculating f_3-statistics for a target composed of a single
987 pseudo-haploid individual is impossible since a heterozygosity estimate is required (Maier
988 et al. 2022), and such singleton groups are common in archaeogenetic studies.
989 Researchers should also be aware that f_3-statistics are defined on unrooted trees, and
990 that may lead to rare but strong false signals of admixture (Fig. S4e).

991

992 ## Methods

993 ### *Simulating random admixture graphs with msprime v.1.1.1*

994 For simulating genetic data, we used *msprime v.1.1.1* which allows accurate simulation of
995 recombination and of multi-chromosome diploid genomes relying on the Wright-Fisher
996 model (Nelson et al. 2020, Baumdicker et al. 2022). We simulated three or ten diploid

997 chromosomes (each 100 Mbp long) by specifying a flat recombination rate (2×10^{-8} per nt per
998 generation) along the chromosome and a much higher rate at the chromosome boundaries
999 ($\log_e 2$ or ~0.693 per nt per generation, see
1000 https://tskit.dev/msprime/docs/stable/ancestry.html#multiple-chromosomes). A flat
1001 mutation rate, 1.25×10^{-8} per nt per generation (Scally & Durbin 2012), and the binary
1002 mutation model were used. To maintain the correct correlation between chromosomes, the
1003 discrete time Wright-Fischer model was used for 25 generations into the past, and deeper in
1004 the past the standard coalescent simulation algorithm was used (as recommended by Nelson
1005 et al. 2020).

1006 Genetic histories in the form of random admixture graphs including 13 populations and 10
1007 pulse-like admixture events were generated using the *random_admixturegraph* and
1008 *random_sim* functions from the *ADMIXTOOLS 2* package
1009 (https://uqrmaie1.github.io/admixtools/reference/random_sim.html), which produced
1010 scripts for running the *msprime v.1.1.1* simulator. Demographic events were separated by
1011 date intervals ranging randomly between 20 and 120 generations, with an upper bound on
1012 the graph depth at 800 generations (or ca. 23,000 years in the case of humans). In another
1013 set of simulations, all the dates were scaled up 3.75 times, with an upper bound on the graph
1014 depth at 3,000 generations (or 87,000 years in the case of humans). To be more precise,
1015 demographic events were not placed in time entirely randomly, but were tied to one or few
1016 other events of the same “topological depth” within the graph, as illustrated by five examples
1017 of the simulated topologies in Fig. S2. The same principle was applied to sampling dates,
1018 which were tied to other demographic events such as divergence and admixture of other
1019 populations. This was done to ensure topological consistency of random graphs.

1020 Ten diploid individuals with no missing data were sampled from each population at "leaves"
1021 of the graph. Effective population sizes were constant along each edge and were picked
1022 randomly from the range of 1,000 – 10,000 diploid individuals. Admixture proportions for all
1023 admixture events varied randomly between 10% and 50%. This setup generates groups
1024 sampled at widely different dates in the past or, in other words, located at various genetic
1025 distances from the root. Alternatively, all terminal branches were extended to the "present"
1026 of the simulation and sampled at "present", keeping their respective effective population

1027 sizes and topological relationships unchanged. Thus, another set of simulations was
1028 generated for the same topologies, where groups were more drifted with respect to each
1029 other (see F_{ST} distributions in Fig. S1).

1030 In summary, four sets of independent simulations differing by the amount of data generated
1031 and by population divergence metrics were performed for a set of 40 random admixture
1032 graph topologies:

1033 1) three 100-Mbp-sized chromosomes; groups sampled at different points in time; maximal
1034 simulated history depth at 800 generations (10 simulation replicates, median number of
1035 polymorphic sites = 669,655, see Fig. S3);

1036 2) ten 100-Mbp-sized chromosomes; groups sampled at different points in time; maximal
1037 simulated history depth at 800 generations (10 simulation replicates, median number of
1038 polymorphic sites = 2,229,459);

1039 3) three 100-Mbp-sized chromosomes; groups sampled at different points in time; maximal
1040 simulated history depth at 3,000 generations (one simulation replicate, median number of
1041 polymorphic sites = 1,074,336);

1042 4) three 100-Mbp-sized chromosomes; all terminal branches extended to the "present" of the
1043 simulation and sampled at that point; maximal simulated history depth at 800 generations
1044 (one simulation replicate, median number of polymorphic sites = 838,297).

1045 To create more realistic datasets, we performed randomised subsampling of polymorphic
1046 sites and individuals (replicates no. 1 of the first and second simulation setups were used for
1047 this, see the list above). First, we randomly sampled alleles at heterozygous sites, creating
1048 pseudo-haploid data. Then we introduced missing data by randomly selecting a missing rate
1049 between 5% and 95%, followed by randomly selecting sites according to the missing rate. This
1050 site subsampling was repeated for each individual independently. Lastly, we randomly
1051 sampled *n* (from 1 to 10) individuals from each population independently. The subsampling
1052 procedure described above was conditioned on the number of sites polymorphic in the set
1053 of 13 simulated populations and was repeated until a subsampling replicate with more than
1054 20,000 (for 300-Mbp-sized genomes) or 66,000 such sites (for 1000-Mbp-sized genomes) was

1055 obtained. We generated 10 independent subsampled replicates for each topology and
1056 simulation setup (800 replicates in total).

1057 Polymorphism data in the *EIGENSTRAT* format were generated from the tree sequences using
1058 the *TreeSequence.genotype_matrix* function (https://tskit.dev/tskit/docs/stable/python-
1059 api.html#tskit.TreeSequence.genotype_matrix) and used for all subsequent analyses (*f*-
1060 statistics and *qpAdm*, PCA, *ADMIXTURE*).

1061 For all the work on *f*-statistics and *qpAdm*, the *ADMIXTOOLS 2* software package (Maier et al.
1062 2022) was used. For diploid SNP sets without missing data, we first calculated all possible f_2-
1063 statistics for 4-Mbp-sized genome blocks (with the "*maxmiss=0*",
1064 "*adjust_pseudohaploid=FALSE*", and "*minac2=FALSE*" settings) and then used them for
1065 calculating f_3- and f_4-statistics as linear combinations of f_2-statistics and for testing *qpAdm*
1066 models using the *qpadm* function in *ADMIXTOOLS 2*
1067 (https://uqrmaie1.github.io/admixtools/) under default settings. Inferred admixture
1068 proportions were not constrained between 0 and 1. For pseudo-haploid SNP sets with missing
1069 data and uneven group sizes, the *qpadm* function was applied directly to genotype files, with
1070 the "*allsnps=TRUE*" setting. In other words, f_4-statistics utilized by *qpAdm* and f_3-statistics
1071 were calculated off the genotype files without intermediate f_2-statistics, and removal of
1072 missing data was done for each population quadruplet or triplet separately. This setup is
1073 often used in the literature in the presence of missing data (e.g., Harney et al. 2018, Harney
1074 et al. 2019, Narasimhan et al. 2019, Lazaridis et al. 2022).

1075

1076 ***Rotating qpAdm protocols***

1077 *QpWave* tests were performed on sets of 13 groups divided randomly into 2 "left" and 11
1078 "right" groups, testing all possible bisections of this form. *QpAdm* was applied to the same
1079 sets of 13 groups divided randomly into 3 "left" and 10 "right" groups, testing all possible
1080 bisections of this form for all possible target groups in "left" sets. This proximal rotating
1081 protocol was applied to all simulation setups. Subsequent work was focused only on feasible
1082 *qpAdm* models defined as follows: 1) *p*-values calculated by *qpWave* for one-way models
1083 "target = proxy source$_1$", "target = proxy source$_2$", and "proxy source$_1$ = proxy source$_2$" are all

1084 below 0.01; 2) in the case of the two-way model "target = proxy source$_1$ + proxy source$_2$",
1085 estimated admixture proportions ± 2 standard errors are between 0 and 1; 3) the *p*-value
1086 calculated by *qpAdm* for the two-way model ≥ 0.01.

1087 For exploring performance of the distal rotating protocol, feasible two-way *qpAdm* models
1088 were simply filtered according to sampling dates of target groups and proxy sources. If target
1089 group's sampling date is equal to or smaller than sampling dates of both proxy sources, such
1090 a model was considered distal.

1091

1092 ***Non-rotating and model competition qpAdm protocols***

1093 In the non-rotating protocol, for each simulated admixture graph six oldest groups were
1094 selected as a fixed "right" set (ties in sampling dates were resolved in alphabetical order;
1095 these "right" sets remained unchanged for a given topology across all independent
1096 simulations), and for the remaining seven groups all possible one-way and two-way
1097 admixture models were tested (105 models), applying the same composite feasibility
1098 criterion that was used above for the rotating protocol. This is the proximal non-rotating
1099 protocol, and alternatively we focused on distal admixture models only (distal non-rotating
1100 protocol).

1101 In the proximal model competition protocol, subsequent analysis was focused on targets for
1102 whom two or more alternative *qpAdm* models emerged as feasible at the first step. For each
1103 target, alternative proxy sources were pooled and rotated between the "left" and "right" sets,
1104 testing only the models that emerged as feasible at the first step and applying the composite
1105 feasibility criterion (*p*-value ≥ 0.01, estimated admixture proportions ± 2 SE are between 0
1106 and 1). Rotation of alternative proxy sources was performed in two alternative ways:
1107 "whatever is not on the left is on the right", or placement of alternative sources in the "right"
1108 set one by one. In the latter case several "right" sets were tested for each model, and the
1109 model was considered supported by the model competition protocol only if it was not
1110 rejected under any of these "right" sets (the latter protocol follows Maróti et al. 2022). If only
1111 one model was feasible for a target, such a model was evaluated as passing the model
1112 competition procedure. A distal model competition protocol was not tested in this study.

1113 For testing statistical significance of differences in FDR between *qpAdm* protocols, the
1114 following approach was used. FDR was calculated either on low-quality data for 10 random
1115 site/individual subsampling replicates derived from simulation replicate no. 1 (simulation
1116 setups no. 1 and 2) or on high-quality data for 10 independent simulation replicates
1117 (simulation setups no. 1 and 2). Comparisons of four *qpAdm* protocols (rotating and non-
1118 rotating, proximal and distal) were performed independently on these four sets of replicates,
1119 using the two-sided paired Wilcoxon test (Table 2). Comparisons of the same *qpAdm* protocol
1120 on lower and higher amounts of data (300-Mbp- vs. 1,000-Mbp-sized simulated genomes)
1121 were performed using the two-sided (non-paired) Wilcoxon test since simulation replicates
1122 were independent unlike alternative *qpAdm* protocols applied to the same data (Table 2).

1123

1124 ***Classifying two-way admixture models into false and true positives***

1125 Since the simulated admixture graph topologies were complex and random, target groups
1126 modelled with *qpAdm* had very complex admixture history in some cases, being a part of
1127 gene flow networks. In this context it is hard to draw a strict boundary between true and false
1128 admixture models composed of a target and only two proxy sources. Two-way admixture
1129 models were considered false only if at least one of the following criteria was satisfied
1130 (considering only graph topologies and admixture proportions):

1131 1. The target and at least one of the proxy sources are simulated as strictly cladal (Fig. 3). In
1132 this case the target may either be unadmixed, or it may have experienced gene flows
1133 earlier in its history that do not break its cladality with one of the proxy sources;
1134 2. A proxy source does not represent any true source. In other words, it is symmetrically
1135 related to all true sources of ancestry in the target (Fig. S4a). Alternatively, both proxy
1136 sources represent the same true source, and are symmetrically related to all the other
1137 true sources (Fig. S4b).
1138 3. A proxy source shares genetic drift with the corresponding true source that is not shared
1139 by the second proxy source (and the same is true for the other proxy source and another
1140 true source, i.e., condition no. 2 above is not satisfied), however less than 40% of its
1141 ancestry is derived from the true source (Fig. S4c);

1142 4. A proxy source lineage is a recipient of gene flow from the target lineage (after the last
1143 admixture event in target's history), possibly mediated by other lineages (Fig. 3, Fig. S4d).
1144 In other words, the incorrect proxy source is a descendant of the target lineage, i.e., the
1145 expected gene flow direction is reversed.

1146 We illustrate these topological rules with five examples of FP and feasible *qpAdm* models in
1147 Fig. 3 and Fig. S4a-e. Two-way models for targets whose population history is best
1148 approximated with three-way and more complex models were considered as true positives if
1149 they included source proxies (that do *not* satisfy the criteria above) for at least two of three
1150 or more true ancestry sources.

1151

1152 ***Principal component analysis***

1153 PCA was performed for one simulation replicate per simulation setup. Prior to the analysis,
1154 linked sites were pruned with *PLINK v.2.00a3LM* (Chang et al. 2015) using the following
1155 settings: window size, 2000 SNPs; window step, 100 SNPs; r^2 threshold = 0.5 (argument "--
1156 indep-pairwise 2000 100 0.5"). PCA was also performed using *PLINK v.2.00a3LM* under
1157 default settings, calculating 10 PCs. Interactive three-dimensional plots visualizing PC1, PC2,
1158 and PC3 were made using the *plotly* R package. A two-way admixture model was considered
1159 supported by PCA if:

1160 1. the target group (the center of the cluster of target individuals, to be precise) lay between
1161 the clusters of proxy source individuals on a straight line in the three-dimensional PC
1162 space;
1163 2. or if it was located at a distance of no more than three target cluster diameters from that
1164 straight line connecting the proxy source clusters.

1165 The second pattern was more common among both TP and FP two-way admixture models:
1166 1.5 and 1.3 times, respectively (across all non-subsampled simulated datasets). This situation
1167 is expected since many targets represent three-way and more complex mixtures, and since
1168 arrangement of populations in the PC space is influenced not only by admixture, but also by
1169 genetic drift.

1170

1171 ***ADMIXTURE analysis***

1172 *ADMIXTURE* analysis was performed for one simulation replicate per simulation setup. Prior
1173 to the analysis, linked sites were pruned with *PLINK v.2.00a3LM* (Chang et al. 2015) using the
1174 following settings: window size, 2000 SNPs; window step, 100 SNPs; r^2 threshold = 0.5
1175 (argument "--indep-pairwise 2000 100 0.5"). *ADMIXTURE v.1.3* (Alexander et al. 2009) was
1176 used in the unsupervised mode under the default settings. The algorithm was run on each
1177 SNP dataset only once, with the number of hypothetical ancestral populations (*K*) ranging
1178 from 3 to 10. This range was selected since the total number of populations in each simulated
1179 history was 13. A two-way admixture model was considered supported by *ADMIXTURE*
1180 analysis if:

1181 1. for at least one *K*, at least 5 of 10 target individuals were modelled as a mixture of at least
1182 two ancestry components, with a minor ancestry component exceeding 2%;
1183 2. typically, ancestry component *A* in the target group was shared with at least 5 individuals
1184 in proxy source 1, but not in proxy source 2, and ancestry component *B* was shared with
1185 at least 5 individuals in proxy source 2, but not in proxy source 1 (see examples in Fig. 3
1186 and Fig. S4); in some cases, both components *A* and *B* were found in the proxy sources,
1187 but in varying proportions;
1188 3. if only one ancestry component in the target was shared with the two proxy sources, the
1189 model was considered unsupported;
1190 4. ancestry components in the target that are absent in any of the sources were ignored
1191 since three-way and more complex admixture histories are common in the set of random
1192 admixture graphs explored here;
1193 5. ancestry components in a proxy source that are absent in the target were also ignored
1194 since a proxy source may not be fully cladal with the real source.

1195 These rules were designed to reproduce typical reasoning of an archaeogeneticist
1196 interpreting *ADMIXTURE* results. Observing a pattern of ancestry components in the target
1197 group and proxy sources compatible with the admixture model "target = proxy source$_1$ +
1198 proxy source$_2$" for one *K* value was enough for declaring that the model is supported by the
1199 *ADMIXTURE* analysis. This condition was motivated by an observation that models supported

at one *K* value only were equally common among FP and TP *qpAdm* models (10% and 13%, respectively, across four simulation setups). Models supported at four or more *K* values were more common among TP *qpAdm* models (3.3% of FP and 12.6% of TP models across four simulation setups).

Probability density curves for radiocarbon and calendar dates

Probability density curves for published radiocarbon and calendar dates were constructed in *OxCal v.4.4*. For calendar dates, we used the *C-Simulate* function in *OxCal v.4.4* for simulating normally distributed dating methods, taking the average calendar date as a median and the length of the timespan as a 95% confidence interval. For radiocarbon dates, we used calibration based on the IntCal20 calibration curve. Probability densities were summarized using the *Sum* function in *OxCal v.4.4* for each of the three groups of individuals, those included in the "left", "right", and "target" population sets in at least one of the published *qpAdm* models (Narasimhan et al. 2019, Lazaridis et al. 2022), and then plotted together.

Acknowledgements

P.F. and P.C. were supported by the Czech Science Foundation (project no. 21-27624S). P.F. was also supported by the John Templeton Foundation (grant no. 61220 to David Reich) and by a gift from Jean-Francois Clin. U.I. and L.A.V. were supported by the Czech Ministry of Education, Youth and Sports (program ERC CZ, project no. LL2103). Computational resources for this work were supplied by the projects "e-INFRA CZ" (no. 90140) and “IT4Innovations National Supercomputing Center” (no. LM2015070) supported by the Ministry of Education, Youth and Sports of the Czech Republic, and by the ELIXIR-CZ project (no. LM2022123), a part of the international ELIXIR infrastructure.

References

1. Alexander DH, Novembre J, Lange K. Fast model-based estimation of ancestry in unrelated

1227 individuals, *Genome Res*. **19** (2009) 1655–1664. doi: 10.1101/gr.094052.109.
1228 2. Allentoft ME, Sikora M, Refoyo-Martínez A, *et al*. Population Genomics of Stone Age Eurasia.
1229 *bioRxiv*. (2022). doi: 10.1101/2022.05.04.490594.
1230 3. Antonio ML, Gao Z, Moots HM, Lucci M, Candilio F, Sawyer S, Oberreiter V, Calderon D,
1231 Devitofranceschi K, Aikens RC, Aneli S, Bartoli F, Bedini A, Cheronet O, Cotter DJ, Fernandes DM,
1232 Gasperetti G, Grifoni R, Guidi A, La Pastina F, Loreti E, Manacorda D, Matullo G, Morretta S,
1233 Nava A, Fiocchi Nicolai V, Nomi F, Pavolini C, Pentiricci M, Pergola P, Piranomonte M, Schmidt R,
1234 Spinola G, Sperduti A, Rubini M, Bondioli L, Coppa A, Pinhasi R, Pritchard JK. Ancient Rome: A
1235 genetic crossroads of Europe and the Mediterranean. *Science*. **366** (2019) 708–714. doi:
1236 10.1126/science.aay6826.
1237 4. Baumdicker F, Bisschop G, Goldstein D, Gower G, Ragsdale AP, Tsambos G, Zhu S, Eldon B,
1238 Ellerman EC, Galloway JG, Gladstein AL, Gorjanc G, Guo B, Jeffery B, Kretzschumar WW, Lohse K,
1239 Matschiner M, Nelson D, Pope NS, Quinto-Cortés CD, Rodrigues MF, Saunack K, Sellinger T,
1240 Thornton K, van Kemenade H, Wohns AW, Wong Y, Gravel S, Kern AD, Koskela J, Ralph PL,
1241 Kelleher J. Efficient ancestry and mutation simulation with msprime 1.0, *Genetics*. **220** (2022)
1242 iyab229. doi: 10.1093/genetics/iyab229.
1243 5. Bergström A, Stanton DWG, Taron UH, Frantz L, Sinding MS, Ersmark E, Pfrengle S, Cassatt-
1244 Johnstone M, Lebrasseur O, Girdland-Flink L, Fernandes DM, Ollivier M, Speidel L,
1245 Gopalakrishnan S, Westbury MV, Ramos-Madrigal J, Feuerborn TR, Reiter E, Gretzinger J, Münzel
1246 SC, Swali P, Conard NJ, Carøe C, Haile J, Linderholm A, Androsov S, Barnes I, Baumann C,
1247 Benecke N, Bocherens H, Brace S, Carden RF, Drucker DG, Fedorov S, Gasparik M, Germonpré M,
1248 Grigoriev S, Groves P, Hertwig ST, Ivanova VV, Janssens L, Jennings RP, Kasparov AK, Kirillova IV,
1249 Kurmaniyazov I, Kuzmin YV, Kosintsev PA, Lázničková-Galetová M, Leduc C, Nikolskiy P,
1250 Nussbaumer M, O'Drisceoil C, Orlando L, Outram A, Pavlova EY, Perri AR, Pilot M, Pitulko VV,
1251 Plotnikov VV, Protopopov AV, Rehazek A, Sablin M, Seguin-Orlando A, Storå J, Verjux C, Zaibert
1252 VF, Zazula G, Crombé P, Hansen AJ, Willerslev E, Leonard JA, Götherström A, Pinhasi R,
1253 Schuenemann VJ, Hofreiter M, Gilbert MTP, Shapiro B, Larson G, Krause J, Dalén L, Skoglund P.
1254 Grey wolf genomic history reveals a dual ancestry of dogs, *Nature*. **607** (2022) 313–320. doi:
1255 10.1038/s41586-022-04824-9.
1256 6. Brielle ES, Fleisher J, Wynne-Jones S, Sirak K, Broomandkhoshbacht N, Callan K, Curtis E, Iliev L,
1257 Lawson AM, Oppenheimer J, Qiu L, Stewardson K, Workman JN, Zalzala F, Ayodo G, Gidna AO,
1258 Kabiru A, Kwekason A, Mabulla AZP, Manthi FK, Ndiema E, Ogola C, Sawchuk E, Al-Gazali L, Ali
1259 BR, Ben-Salem S, Letellier T, Pierron D, Radimilahy C, Rakotoarisoa JA, Raaum RL, Culleton BJ,
1260 Mallick S, Rohland N, Patterson N, Mwenje MA, Ahmed KB, Mohamed MM, Williams SR, Monge

J, Kusimba S, Prendergast ME, Reich D, Kusimba CM. Entwined African and Asian genetic roots of medieval peoples of the Swahili coast. *Nature*. **615** (2023) 866–873. doi: 10.1038/s41586-023-05754-w.

7. Carlhoff S, Duli A, Nägele K, Nur M, Skov L, Sumantri I, Oktaviana AA, Hakim B, Burhan B, Syahdar FA, McGahan DP, Bulbeck D, Perston YL, Newman K, Saiful AM, Ririmasse M, Chia S, Hasanuddin, Pulubuhu DAT, Suryatman, Supriadi, Jeong C, Peter BM, Prüfer K, Powell A, Krause J, Posth C, Brumm A. Genome of a middle Holocene hunter-gatherer from Wallacea. *Nature*. **596** (2021) 543–547. doi: 10.1038/s41586-021-03823-6.
8. Chang CC, Chow CC, Tellier LC, Vattikuti S, Purcell SM, Lee JJ. Second-generation PLINK: rising to the challenge of larger and richer datasets, *Gigascience*. **4** (2015) 7. doi: 10.1186/s13742-015-0047-8.
9. Changmai P, Jaisamut K, Kampuansai J, Kutanan W, Altınışık NE, Flegontova O, Inta A, Yüncü E, Boonthai W, Pamjav H, Reich D, Flegontov P. Indian genetic heritage in Southeast Asian populations, *PLoS Genet*. **18** (2022a) e1010036. doi: 10.1371/journal.pgen.1010036.
10. Changmai P, Pinhasi R, Pietrusewsky M, Stark MT, Ikehara-Quebral RM, Reich D, Flegontov P. Ancient DNA from Protohistoric Period Cambodia indicates that South Asians admixed with local populations as early as 1st-3rd centuries CE, *Sci. Rep*. **12** (2022b) 22507. doi: 10.1038/s41598-022-26799-3.
11. Chintalapati M, Patterson N, Moorjani P. The spatiotemporal patterns of major human admixture events during the European Holocene, *eLife*. **11** (2022) e77625. doi: 10.7554/eLife.77625.
12. de Barros Damgaard P, Martiniano R, Kamm J, Moreno-Mayar JV, Kroonen G, Peyrot M, Barjamovic G, Rasmussen S, Zacho C, Baimukhanov N, Zaibert V, Merz V, Biddanda A, Merz I, Loman V, Evdokimov V, Usmanova E, Hemphill B, Seguin-Orlando A, Yediay FE, Ullah I, Sjögren KG, Iversen KH, Choin J, de la Fuente C, Ilardo M, Schroeder H, Moiseyev V, Gromov A, Polyakov A, Omura S, Senyurt SY, Ahmad H, McKenzie C, Margaryan A, Hameed A, Samad A, Gul N, Khokhar MH, Goriunova OI, Bazaliiskii VI, Novembre J, Weber AW, Orlando L, Allentoft ME, Nielsen R, Kristiansen K, Sikora M, Outram AK, Durbin R, Willerslev E. The first horse herders and the impact of early Bronze Age steppe expansions into Asia, *Science*. **360** (2018) eaar7711. doi: 10.1126/science.aar7711.
13. Durand EY, Patterson N, Reich D, Slatkin M. Testing for ancient admixture between closely related populations, *Mol. Biol. Evol*. **28** (2011) 2239–2252. doi: 10.1093/molbev/msr048.
14. Fernandes DM, Mittnik A, Olalde I, Lazaridis I, Cheronet O, Rohland N, Mallick S, Bernardos R, Broomandkhoshbacht N, Carlsson J, Culleton BJ, Ferry M, Gamarra B, Lari M, Mah M, Michel M,

Modi A, Novak M, Oppenheimer J, Sirak KA, Stewardson K, Mandl K, Schattke C, Özdoğan KT, Lucci M, Gasperetti G, Candilio F, Salis G, Vai S, Camarós E, Calò C, Catalano G, Cueto M, Forgia V, Lozano M, Marini E, Micheletti M, Miccichè RM, Palombo MR, Ramis D, Schimmenti V, Sureda P, Teira L, Teschler-Nicola M, Kennett DJ, Lalueza-Fox C, Patterson N, Sineo L, Coppa A, Caramelli D, Pinhasi R, Reich D. The spread of steppe and Iranian-related ancestry in the islands of the western Mediterranean, *Nat. Ecol. Evol*. **4** (2020) 334–345. doi: 10.1038/s41559-020-1102-0.

15. Fernandes DM, Sirak KA, Ringbauer H, Sedig J, Rohland N, Cheronet O, Mah M, Mallick S, Olalde I, Culleton BJ, Adamski N, Bernardos R, Bravo G, Broomandkhoshbacht N, Callan K, Candilio F, Demetz L, Carlson KSD, Eccles L, Freilich S, George RJ, Lawson AM, Mandl K, Marzaioli F, McCool WC, Oppenheimer J, Özdogan KT, Schattke C, Schmidt R, Stewardson K, Terrasi F, Zalzala F, Antúnez CA, Canosa EV, Colten R, Cucina A, Genchi F, Kraan C, La Pastina F, Lucci M, Maggiolo MV, Marcheco-Teruel B, Maria CT, Martínez C, París I, Pateman M, Simms TM, Sivoli CG, Vilar M, Kennett DJ, Keegan WF, Coppa A, Lipson M, Pinhasi R, Reich D. A genetic history of the pre-contact Caribbean, *Nature*. **590** (2021) 103–110. doi: 10.1038/s41586-020-03053-2.
16. Frichot E, Schoville S, Bouchard G, François O. Correcting principal component maps for effects of spatial autocorrelation in population genetic data, *Front. Genet*. **3** (2012) 254. doi: 10.3389/fgene.2012.00254.
17. Furtwängler A, Rohrlach AB, Lamnidis TC, Papac L, Neumann GU, Siebke I, Reiter E, Steuri N, Hald J, Denaire A, Schnitzler B, Wahl J, Ramstein M, Schuenemann VJ, Stockhammer PW, Hafner A, Lösch S, Haak W, Schiffels S, Krause J. Ancient genomes reveal social and genetic structure of Late Neolithic Switzerland. *Nat. Commun*. **11** (2020) 1915. doi: 10.1038/s41467-020-15560-x.
18. Green RE, Krause J, Briggs AW, Maricic T, Stenzel U, Kircher M, Patterson N, Li H, Zhai W, Fritz MH, Hansen NF, Durand EY, Malaspinas AS, Jensen JD, Marques-Bonet T, Alkan C, Prüfer K, Meyer M, Burbano HA, Good JM, Schultz R, Aximu-Petri A, Butthof A, Höber B, Höffner B, Siegemund M, Weihmann A, Nusbaum C, Lander ES, Russ C, Novod N, Affourtit J, Egholm M, Verna C, Rudan P, Brajkovic D, Kucan Ž, Gušic I, Doronichev VB, Golovanova LV, Lalueza-Fox C, de la Rasilla M, Fortea J, Rosas A, Schmitz RW, Johnson PLF, Eichler EE, Falush D, Birney E, Mullikin JC, Slatkin M, Nielsen R, Kelso J, Lachmann M, Reich D, Pääbo S. A draft sequence of the Neandertal genome, *Science*. **328** (2010) 710–722. doi: 10.1126/science.1188021.
19. Gnecchi-Ruscone GA, Szécsényi-Nagy A, Koncz I, Csiky G, Rácz Z, Rohrlach AB, Brandt G, Rohland N, Csáky V, Cheronet O, Szeifert B, Rácz TÁ, Benedek A, Bernert Z, Berta N, Czifra S, Dani J, Farkas Z, Hága T, Hajdu T, Jászberényi M, Kisjuhász V, Kolozsi B, Major P, Marcsik A, Kovacsóczy BN, Balogh C, Lezsák GM, Ódor JG, Szelekovszky M, Szeniczey T, Tárnoki J, Tóth Z, Tutkovics EK, Mende BG, Geary P, Pohl W, Vida T, Pinhasi R, Reich D, Hofmanová Z, Jeong C, Krause J. Ancient

genomes reveal origin and rapid trans-Eurasian migration of 7th century Avar elites, *Cell*. **185** (2022) 1402–1413.e21. doi: 10.1016/j.cell.2022.03.007.

20. Haak W, Lazaridis I, Patterson N, Rohland N, Mallick S, Llamas B, Brandt G, Nordenfelt S, Harney E, Stewardson K, Fu Q, Mittnik A, Bánffy E, Economou C, Francken M, Friederich S, Pena RG, Hallgren F, Khartanovich V, Khokhlov A, Kunst M, Kuznetsov P, Meller H, Mochalov O, Moiseyev V, Nicklisch N, Pichler SL, Risch R, Rojo Guerra MA, Roth C, Szécsényi-Nagy A, Wahl J, Meyer M, Krause J, Brown D, Anthony D, Cooper A, Alt KW, Reich D. Massive migration from the steppe was a source for Indo-European languages in Europe, *Nature*. **522** (2015) 207–211. doi: 10.1038/nature14317.
21. Harney É, May H, Shalem D, Rohland N, Mallick S, Lazaridis I, Sarig R, Stewardson K, Nordenfelt S, Patterson N, Hershkovitz I, Reich D. Ancient DNA from Chalcolithic Israel reveals the role of population mixture in cultural transformation, *Nat. Commun*. **9** (2018) 3336. doi: 10.1038/s41467-018-05649-9.
22. Harney É, Nayak A, Patterson N, Joglekar P, Mushrif-Tripathy V, Mallick S, Rohland N, Sedig J, Adamski N, Bernardos R, Broomandkhoshbacht N, Culleton BJ, Ferry M, Harper TK, Michel M, Oppenheimer J, Stewardson K, Zhang Z, Harashawaradhana, Bartwal MS, Kumar S, Diyundi SC, Roberts P, Boivin N, Kennett DJ, Thangaraj K, Reich D, Rai N. Ancient DNA from the skeletons of Roopkund Lake reveals Mediterranean migrants in India, *Nat. Commun*. **10** (2019) 3670. doi: 10.1038/s41467-019-11357-9.
23. Harney É, Patterson N, Reich D, Wakeley J. Assessing the performance of qpAdm: a statistical tool for studying population admixture, *Genetics*. **217** (2021) iyaa045. doi: 10.1093/GENETICS/IYAA045.
24. Jeong C, Balanovsky O, Lukianova E, Kahbatkyzy N, Flegontov P, Zaporozhchenko V, Immel A, Wang CC, Ixan O, Khussainova E, Bekmanov B, Zaibert V, Lavryashina M, Pocheshkhova E, Yusupov Y, Agdzhoyan A, Koshel S, Bukin A, Nymadawa P, Turdikulova S, Dalimova D, Churnosov M, Skhalyakho R, Daragan D, Bogunov Y, Bogunova A, Shtrunov A, Dubova N, Zhabagin M, Yepiskoposyan L, Churakov V, Pislegin N, Damba L, Saroyants L, Dibirova K, Atramentova L, Utevska O, Idrisov E, Kamenshchikova E, Evseeva I, Metspalu M, Outram AK, Robbeets M, Djansugurova L, Balanovska E, Schiffels S, Haak W, Reich D, Krause J. The genetic history of admixture across inner Eurasia, *Nat. Ecol. Evol*. **3** (2019) 966–976. doi: 10.1038/s41559-019-0878-2.
25. Lawson DJ, van Dorp L, Falush D. A tutorial on how not to over-interpret STRUCTURE and ADMIXTURE bar plots, *Nat Commun*. **9** (2018) 3258. doi: 10.1038/s41467-018-05257-7.
26. Lazaridis I, Nadel D, Rollefson G, Merrett DC, Rohland N, Mallick S, Fernandes D, Novak M,

Gamarra B, Sirak K, Connell S, Stewardson K, Harney E, Fu Q, Gonzalez-Fortes G, Jones ER, Roodenberg SA, Lengyel G, Bocquentin F, Gasparian B, Monge JM, Gregg M, Eshed V, Mizrahi AS, Meiklejohn C, Gerritsen F, Bejenaru L, Blüher M, Campbell A, Cavalleri G, Comas D, Froguel P, Gilbert E, Kerr SM, Kovacs P, Krause J, McGettigan D, Merrigan M, Merriwether DA, O'Reilly S, Richards MB, Semino O, Shamoon-Pour M, Stefanescu G, Stumvoll M, Tönjes A, Torroni A, Wilson JF, Yengo L, Hovhannisyan NA, Patterson N, Pinhasi R, Reich D. Genomic insights into the origin of farming in the ancient Near East, *Nature*. **536** (2016) 419–424. doi: 10.1038/nature19310.

27. Lazaridis I, Mittnik A, Patterson N, Mallick S, Rohland N, Pfrengle S, Furtwängler A, Peltzer A, Posth C, Vasilakis A, McGeorge PJP, Konsolaki-Yannopoulou E, Korres G, Martlew H, Michalodimitrakis M, Özsait M, Özsait N, Papathanasiou A, Richards M, Roodenberg SA, Tzedakis Y, Arnott R, Fernandes DM, Hughey JR, Lotakis DM, Navas PA, Maniatis Y, Stamatoyannopoulos JA, Stewardson K, Stockhammer P, Pinhasi R, Reich D, Krause J, Stamatoyannopoulos G. Genetic origins of the Minoans and Mycenaeans, *Nature*. **548** (2017) 214–218. doi: 10.1038/nature23310.

28. Lazaridis I, Alpaslan-Roodenberg S, Acar A, Açıkkol A, Agelarakis A, Aghikyan L, Akyüz U, Andreeva D, Andrijašević G, Antonović D, Armit I, Atmaca A, Avetisyan P, Aytek Aİ, Bacvarov K, Badalyan R, Bakardzhiev S, Balen J, Bejko L, Bernardos R, Bertsatos A, Biber H, Bilir A, Bodružić M, Bonogofsky M, Bonsall C, Borić D, Borovinić N, Bravo Morante G, Buttinger K, Callan K, Candilio F, Carić M, Cheronet O, Chohadzhiev S, Chovalopoulou ME, Chryssoulaki S, Ciobanu I, Čondić N, Constantinescu M, Cristiani E, Culleton BJ, Curtis E, Davis J, Demcenco TI, Dergachev V, Derin Z, Deskaj S, Devejyan S, Djordjević V, Duffett Carlson KS, Eccles LR, Elenski N, Engin A, Erdoğan N, Erir-Pazarcı S, Fernandes DM, Ferry M, Freilich S, Frînculeasa A, Galaty ML, Gamarra B, Gasparyan B, Gaydarska B, Genç E, Gültekin T, Gündüz S, Hajdu T, Heyd V, Hobosyan S, Hovhannisyan N, Iliev I, Iliev L, Iliev S, İvgin İ, Janković I, Jovanova L, Karkanas P, Kavaz-Kındığılı B, Kaya EH, Keating D, Kennett DJ, Deniz Kesici S, Khudaverdyan A, Kiss K, Kılıç S, Klostermann P, Kostak Boca Negra Valdes S, Kovačević S, Krenz-Niedbała M, Krznarić Škrivanko M, Kurti R, Kuzman P, Lawson AM, Lazar C, Leshtakov K, Levy TE, Liritzis I, Lorentz KO, Łukasik S, Mah M, Mallick S, Mandl K, Martirosyan-Olshansky K, Matthews R, Matthews W, McSweeney K, Melikyan V, Micco A, Michel M, Milašinović L, Mittnik A, Monge JM, Nekhrizov G, Nicholls R, Nikitin AG, Nikolov V, Novak M, Olalde I, Oppenheimer J, Osterholtz A, Özdemir C, Özdoğan KT, Öztürk N, Papadimitriou N, Papakonstantinou N, Papathanasiou A, Paraman L, Paskary EG, Patterson N, Petrakiev I, Petrosyan L, Petrova V, Philippa-Touchais A, Piliposyan A, Pocuca Kuzman N, Potrebica H, Preda-Bălănică B, Premužić Z, Price TD, Qiu L, Radović S, Raeuf Aziz K,

Rajić Šikanjić P, Rasheed Raheem K, Razumov S, Richardson A, Roodenberg J, Ruka R, Russeva V, Şahin M, Şarbak A, Savaş E, Schattke C, Schepartz L, Selçuk T, Sevim-Erol A, Shamoon-Pour M, Shephard HM, Sideris A, Simalcsik A, Simonyan H, Sinika V, Sirak K, Sirbu G, Šlaus M, Soficaru A, Söğüt B, Sołtysiak A, Sönmez-Sözer Ç, Stathi M, Steskal M, Stewardson K, Stocker S, Suata-Alpaslan F, Suvorov A, Szécsényi-Nagy A, Szeniczey T, Telnov N, Temov S, Todorova N, Tota U, Touchais G, Triantaphyllou S, Türker A, Ugarković M, Valchev T, Veljanovska F, Videvski Z, Virag C, Wagner A, Walsh S, Włodarczak P, Workman JN, Yardumian A, Yarovoy E, Yavuz AY, Yılmaz H, Zalzala F, Zettl A, Zhang Z, Çavuşoğlu R, Rohland N, Pinhasi R, Reich D, Davtyan R. The genetic history of the Southern Arc: A bridge between West Asia and Europe, *Science*. **377** (2022) eabm4247. doi: 10.1126/science.abm4247.

29. Lee J, Miller BK, Bayarsaikhan J, Johannesson E, Ventresca Miller A, Warinner C, Jeong C. Genetic population structure of the Xiongnu Empire at imperial and local scales. *Sci. Adv*. **9** (2023) eadf3904. doi: 10.1126/sciadv.adf3904.

30. Librado P, Khan N, Fages A, Kusliy MA, Suchan T, Tonasso-Calvière L, Schiavinato S, Alioglu D, Fromentier A, Perdereau A, Aury JM, Gaunitz C, Chauvey L, Seguin-Orlando A, Der Sarkissian C, Southon J, Shapiro B, Tishkin AA, Kovalev AA, Alquraishi S, Alfarhan AH, Al-Rasheid KAS, Seregély T, Klassen L, Iversen R, Bignon-Lau O, Bodu P, Olive M, Castel JC, Boudadi-Maligne M, Alvarez N, Germonpré M, Moskal-Del Hoyo M, Wilczyński J, Pospuła S, Lasota-Kuś A, Tunia K, Nowak M, Rannamäe E, Saarma U, Boeskorov G, Lõugas L, Kyselý R, Peške L, Bălășescu A, Dumitrașcu V, Dobrescu R, Gerber D, Kiss V, Szécsényi-Nagy A, Mende BG, Gallina Z, Somogyi K, Kulcsár G, Gál E, Bendrey R, Allentoft ME, Sirbu G, Dergachev V, Shephard H, Tomadini N, Grouard S, Kasparov A, Basilyan AE, Anisimov MA, Nikolskiy PA, Pavlova EY, Pitulko V, Brem G, Wallner B, Schwall C, Keller M, Kitagawa K, Bessudnov AN, Bessudnov A, Taylor W, Magail J, Gantulga JO, Bayarsaikhan J, Erdenebaatar D, Tabaldiev K, Mijiddorj E, Boldgiv B, Tsagaan T, Pruvost M, Olsen S, Makarewicz CA, Valenzuela Lamas S, Albizuri Canadell S, Nieto Espinet A, Iborra MP, Lira Garrido J, Rodríguez González E, Celestino S, Olària C, Arsuaga JL, Kotova N, Pryor A, Crabtree P, Zhumatayev R, Toleubaev A, Morgunova NL, Kuznetsova T, Lordkipanize D, Marzullo M, Prato O, Bagnasco Gianni G, Tecchiati U, Clavel B, Lepetz S, Davoudi H, Mashkour M, Berezina NY, Stockhammer PW, Krause J, Haak W, Morales-Muñiz A, Benecke N, Hofreiter M, Ludwig A, Graphodatsky AS, Peters J, Kiryushin KY, Iderkhangai TO, Bokovenko NA, Vasiliev SK, Seregin NN, Chugunov KV, Plasteeva NA, Baryshnikov GF, Petrova E, Sablin M, Ananyevskaya E, Logvin A, Shevnina I, Logvin V, Kalieva S, Loman V, Kukushkin I, Merz I, Merz V, Sakenov S, Varfolomeyev V, Usmanova E, Zaibert V, Arbuckle B, Belinskiy AB, Kalmykov A, Reinhold S, Hansen S, Yudin AI, Vybornov AA, Epimakhov A, Berezina NS, Roslyakova N, Kosintsev PA, Kuznetsov PF, Anthony D,

Kroonen GJ, Kristiansen K, Wincker P, Outram A, Orlando L. The origins and spread of domestic horses from the Western Eurasian steppes, *Nature*. **598** (2021) 634–640. doi: 10.1038/s41586-021-04018-9.

31. Lipson M. Applying f_4-statistics and admixture graphs: Theory and examples, *Mol. Ecol. Resour*. **20** (2020) 1658–1667. doi: 10.1111/1755-0998.13230.
32. Loh PR, Lipson M, Patterson N, Moorjani P, Pickrell JK, Reich D, Berger B. Inferring admixture histories of human populations using linkage disequilibrium, *Genetics*. **193** (2013) 1233–1254. doi: 10.1534/genetics.112.147330.
33. Maier R, Flegontov P, Flegontova O, Işıldak U, Changmai P, Reich D. On the limits of fitting complex models of population history to *f*-statistics. *eLife*. **12** (2023) e85492. doi: 10.7554/eLife.85492.
34. Maróti Z, Neparáczki E, Schütz O, Maár K, Varga GIB, Kovács B, Kalmár T, Nyerki E, Nagy I, Latinovics D, Tihanyi B, Marcsik A, Pálfi G, Bernert Z, Gallina Z, Horváth C, Varga S, Költő L, Raskó I, Nagy PL, Balogh C, Zink A, Maixner F, Götherström A, George R, Szalontai C, Szenthe G, Gáll E, Kiss AP, Gulyás B, Kovacsóczy BN, Gál SS, Tomka P, Török T. The genetic origin of Huns, Avars, and conquering Hungarians, *Curr. Biol*. **32** (2022) 2858–2870.e7. doi: 10.1016/j.cub.2022.04.093.
35. Martin SH, Davey JW, Jiggins CD. Evaluating the use of ABBA-BABA statistics to locate introgressed loci, *Mol. Biol. Evol*. **32** (2014) 244–257. doi: 10.1093/molbev/msu269.
36. Marcus JH, Posth C, Ringbauer H, Lai L, Skeates R, Sidore C, Beckett J, Furtwängler A, Olivieri A, Chiang CWK, Al-Asadi H, Dey K, Joseph TA, Liu CC, Der Sarkissian C, Radzevičiūtė R, Michel M, Gradoli MG, Marongiu P, Rubino S, Mazzarello V, Rovina D, La Fragola A, Serra RM, Bandiera P, Bianucci R, Pompianu E, Murgia C, Guirguis M, Orquin RP, Tuross N, van Dommelen P, Haak W, Reich D, Schlessinger D, Cucca F, Krause J, Novembre J. Genetic history from the Middle Neolithic to present on the Mediterranean island of Sardinia, *Nat. Commun*. **11** (2020) 939. doi: 10.1038/s41467-020-14523-6.
37. Maróti Z, Neparáczki E, Schütz O, Maár K, Varga GIB, Kovács B, Kalmár T, Nyerki E, Nagy I, Latinovics D, Tihanyi B, Marcsik A, Pálfi G, Bernert Z, Gallina Z, Horváth C, Varga S, Költő L, Raskó I, Nagy PL, Balogh C, Zink A, Maixner F, Götherström A, George R, Szalontai C, Szenthe G, Gáll E, Kiss AP, Gulyás B, Kovacsóczy BN, Gál SS, Tomka P, Török T. The genetic origin of Huns, Avars, and conquering Hungarians, *Curr. Biol*. **32** (2022) 2858–2870.e7. doi: 10.1016/j.cub.2022.04.093.
38. Mathieson I, Lazaridis I, Rohland N, Mallick S, Patterson N, Roodenberg SA, Harney E, Stewardson K, Fernandes D, Novak M, Sirak K, Gamba C, Jones ER, Llamas B, Dryomov S, Pickrell J, Arsuaga JL, de Castro JM, Carbonell E, Gerritsen F, Khokhlov A, Kuznetsov P, Lozano M, Meller H, Mochalov O, Moiseyev V, Guerra MA, Roodenberg J, Vergès JM, Krause J, Cooper A, Alt KW,

Brown D, Anthony D, Lalueza-Fox C, Haak W, Pinhasi R, Reich D. Genome-wide patterns of selection in 230 ancient Eurasians, *Nature*. **528** (2015) 499–503. doi: 10.1038/nature16152. Epub 2015 Nov 23. PMID: 26595274; PMCID: PMC4918750.

39. Mathieson I, Alpaslan-Roodenberg S, Posth C, Szécsényi-Nagy A, Rohland N, Mallick S, Olalde I, Broomandkhoshbacht N, Candilio F, Cheronet O, Fernandes D, Ferry M, Gamarra B, Fortes GG, Haak W, Harney E, Jones E, Keating D, Krause-Kyora B, Kucukkalipci I, Michel M, Mittnik A, Nägele K, Novak M, Oppenheimer J, Patterson N, Pfrengle S, Sirak K, Stewardson K, Vai S, Alexandrov S, Alt KW, Andreescu R, Antonović D, Ash A, Atanassova N, Bacvarov K, Gusztáv MB, Bocherens H, Bolus M, Boroneanţ A, Boyadzhiev Y, Budnik A, Burmaz J, Chohadzhiev S, Conard NJ, Cottiaux R, Čuka M, Cupillard C, Drucker DG, Elenski N, Francken M, Galabova B, Ganetsovski G, Gély B, Hajdu T, Handzhyiska V, Harvati K, Higham T, Iliev S, Janković I, Karavanić I, Kennett DJ, Komšo D, Kozak A, Labuda D, Lari M, Lazar C, Leppek M, Leshtakov K, Vetro DL, Los D, Lozanov I, Malina M, Martini F, McSweeney K, Meller H, Menđušić M, Mirea P, Moiseyev V, Petrova V, Price TD, Simalcsik A, Sineo L, Šlaus M, Slavchev V, Stanev P, Starović A, Szeniczey T, Talamo S, Teschler-Nicola M, Thevenet C, Valchev I, Valentin F, Vasilyev S, Veljanovska F, Venelinova S, Veselovskaya E, Viola B, Virag C, Zaninović J, Zäuner S, Stockhammer PW, Catalano G, Krauß R, Caramelli D, Zariņa G, Gaydarska B, Lillie M, Nikitin AG, Potekhina I, Papathanasiou A, Borić D, Bonsall C, Krause J, Pinhasi R, Reich D. The genomic history of southeastern Europe, *Nature*. **555** (2018) 197–203. doi: 10.1038/nature25778.

40. McVean G. A genealogical interpretation of principal components analysis, *PLoS Genet*. **5** (2009) e1000686. doi: 10.1371/journal.pgen.1000686.

41. Moreno-Mayar JV, Potter BA, Vinner L, Steinrücken M, Rasmussen S, Terhorst J, Kamm JA, Albrechtsen A, Malaspinas AS, Sikora M, Reuther JD, Irish JD, Malhi RS, Orlando L, Song YS, Nielsen R, Meltzer DJ, Willerslev E. Terminal Pleistocene Alaskan genome reveals first founding population of Native Americans. *Nature*. **553** (2018a) 203–207. doi: 10.1038/nature25173.

42. Moreno-Mayar JV, Vinner L, de Barros Damgaard P, de la Fuente C, Chan J, Spence JP, Allentoft ME, Vimala T, Racimo F, Pinotti T, Rasmussen S, Margaryan A, Iraeta Orbegozo M, Mylopotamitaki D, Wooller M, Bataille C, Becerra-Valdivia L, Chivall D, Comeskey D, Devièse T, Grayson DK, George L, Harry H, Alexandersen V, Primeau C, Erlandson J, Rodrigues-Carvalho C, Reis S, Bastos MQR, Cybulski J, Vullo C, Morello F, Vilar M, Wells S, Gregersen K, Hansen KL, Lynnerup N, Mirazón Lahr M, Kjær K, Strauss A, Alfonso-Durruty M, Salas A, Schroeder H, Higham T, Malhi RS, Rasic JT, Souza L, Santos FR, Malaspinas AS, Sikora M, Nielsen R, Song YS, Meltzer DJ, Willerslev E. Early human dispersals within the Americas, *Science*. **362** (2018b) eaav2621. doi: 10.1126/science.aav2621.

1499 43. Narasimhan VM, Patterson N, Moorjani P, Rohland N, Bernardos R, Mallick S, Lazaridis I,
1500 Nakatsuka N, Olalde I, Lipson M, Kim AM, Olivieri LM, Coppa A, Vidale M, Mallory J, Moiseyev V,
1501 Kitov E, Monge J, Adamski N, Alex N, Broomandkhoshbacht N, Candilio F, Callan K, Cheronet O,
1502 Culleton BJ, Ferry M, Fernandes D, Freilich S, Gamarra B, Gaudio D, Hajdinjak M, Harney É,
1503 Harper TK, Keating D, Lawson AM, Mah M, Mandl K, Michel M, Novak M, Oppenheimer J, Rai N,
1504 Sirak K, Slon V, Stewardson K, Zalzala F, Zhang Z, Akhatov G, Bagashev AN, Bagnera A,
1505 Baitanayev B, Bendezu-Sarmiento J, Bissembaev AA, Bonora GL, Chargynov TT, Chikisheva T,
1506 Dashkovskiy PK, Derevianko A, Dobeš M, Douka K, Dubova N, Duisengali MN, Enshin D,
1507 Epimakhov A, Fribus AV, Fuller D, Goryachev A, Gromov A, Grushin SP, Hanks B, Judd M, Kazizov
1508 E, Khokhlov A, Krygin AP, Kupriyanova E, Kuznetsov P, Luiselli D, Maksudov F, Mamedov AM,
1509 Mamirov TB, Meiklejohn C, Merrett DC, Micheli R, Mochalov O, Mustafokulov S, Nayak A,
1510 Pettener D, Potts R, Razhev D, Rykun M, Sarno S, Savenkova TM, Sikhymbaeva K, Slepchenko
1511 SM, Soltobaev OA, Stepanova N, Svyatko S, Tabaldiev K, Teschler-Nicola M, Tishkin AA, Tkachev
1512 VV, Vasilyev S, Velemínský P, Voyakin D, Yermolayeva A, Zahir M, Zubkov VS, Zubova A, Shinde
1513 VS, Lalueza-Fox C, Meyer M, Anthony D, Boivin N, Thangaraj K, Kennett DJ, Frachetti M, Pinhasi
1514 R, Reich D. The formation of human populations in South and Central Asia, *Science*. **365** (2019)
1515 eaat7487. doi: 10.1126/science.aat7487.
1516 44. Nelson D, Kelleher J, Ragsdale AP, Moreau C, McVean G, Gravel S. Accounting for long-range
1517 correlations in genome-wide simulations of large cohorts, *PLoS Genet*. **16** (2020) e1008619. doi:
1518 10.1371/journal.pgen.1008619.
1519 45. Ning C, Li T, Wang K, Zhang F, Li T, Wu X, Gao S, Zhang Q, Zhang H, Hudson MJ, Dong G, Wu S,
1520 Fang Y, Liu C, Feng C, Li W, Han T, Li R, Wei J, Zhu Y, Zhou Y, Wang CC, Fan S, Xiong Z, Sun Z, Ye
1521 M, Sun L, Wu X, Liang F, Cao Y, Wei X, Zhu H, Zhou H, Krause J, Robbeets M, Jeong C, Cui Y.
1522 Ancient genomes from northern China suggest links between subsistence changes and human
1523 migration, *Nat. Commun*. **11** (2020) 2700. doi: 10.1038/s41467-020-16557-2.
1524 46. Ning C, Fernandes D, Changmai P, Flegontova O, Yüncü E, Maier R, Altınışık NE, Kassian AS,
1525 Krause J., Lalueza-Fox C, Manica A, Potter BA, Robbeets M, Sirak K, Siska V, Vajda EJ, Vyazov LA,
1526 Wang K, Wang L, Wu X, Xiao X, Zhang F, Reich D, Schiffels S, Pinhasi R, Cui Y, Flegontov P. The
1527 genomic formation of First American ancestors in East and Northeast Asia, *bioRxiv*. (2020). doi:
1528 10.1101/2020.10.12.336628.
1529 47. Novembre J, Stephens M. Interpreting principal component analyses of spatial population
1530 genetic variation, *Nat. Genet*. **40** (2008) 646–649. doi: 10.1038/ng.139.
1531 48. Olalde I, Mallick S, Patterson N, Rohland N, Villalba-Mouco V, Silva M, Dulias K, Edwards CJ,
1532 Gandini F, Pala M, Soares P, Ferrando-Bernal M, Adamski N, Broomandkhoshbacht N, Cheronet

O, Culleton BJ, Fernandes D, Lawson AM, Mah M, Oppenheimer J, Stewardson K, Zhang Z, Jiménez Arenas JM, Toro Moyano IJ, Salazar-García DC, Castanyer P, Santos M, Tremoleda J, Lozano M, García Borja P, Fernández-Eraso J, Mujika-Alustiza JA, Barroso C, Bermúdez FJ, Viguera Mínguez E, Burch J, Coromina N, Vivó D, Cebrià A, Fullola JM, García-Puchol O, Morales JI, Oms FX, Majó T, Vergès JM, Díaz-Carvajal A, Ollich-Castanyer I, López-Cachero FJ, Silva AM, Alonso-Fernández C, Delibes de Castro G, Jiménez Echevarría J, Moreno-Márquez A, Pascual Berlanga G, Ramos-García P, Ramos-Muñoz J, Vijande Vila E, Aguilella Arzo G, Esparza Arroyo Á, Lillios KT, Mack J, Velasco-Vázquez J, Waterman A, Benítez de Lugo Enrich L, Benito Sánchez M, Agustí B, Codina F, de Prado G, Estalrrich A, Fernández Flores Á, Finlayson C, Finlayson G, Finlayson S, Giles-Guzmán F, Rosas A, Barciela González V, García Atiénzar G, Hernández Pérez MS, Llanos A, Carrión Marco Y, Collado Beneyto I, López-Serrano D, Sanz Tormo M, Valera AC, Blasco C, Liesau C, Ríos P, Daura J, de Pedro Michó MJ, Diez-Castillo AA, Flores Fernández R, Francès Farré J, Garrido-Pena R, Gonçalves VS, Guerra-Doce E, Herrero-Corral AM, Juan-Cabanilles J, López-Reyes D, McClure SB, Merino Pérez M, Oliver Foix A, Sanz Borràs M, Sousa AC, Vidal Encinas JM, Kennett DJ, Richards MB, Werner Alt K, Haak W, Pinhasi R, Lalueza-Fox C, Reich D. The genomic history of the Iberian Peninsula over the past 8000 years, *Science*. **363** (2019) 1230–1234. doi: 10.1126/science.aav4040.

49. Oliveira S, Nägele K, Carlhoff S, Pugach I, Koesbardiati T, Hübner A, Meyer M, Oktaviana AA, Takenaka M, Katagiri C, Murti DB, Putri RS, Mahirta, Petchey F, Higham T, Higham CFW, O'Connor S, Hawkins S, Kinaston R, Bellwood P, Ono R, Powell A, Krause J, Posth C, Stoneking M. Ancient genomes from the last three millennia support multiple human dispersals into Wallacea. *Nat. Ecol. Evol*. **6** (2022) 1024–1034. doi: 10.1038/s41559-022-01775-2.

50. Papac L, Ernée M, Dobeš M, Langová M, Rohrlach AB, Aron F, Neumann GU, Spyrou MA, Rohland N, Velemínský P, Kuna M, Brzobohatá H, Culleton B, Daněček D, Danielisová A, Dobisíková M, Hložek J, Kennett DJ, Klementová J, Kostka M, Krištuf P, Kuchařík M, Hlavová JK, Limburský P, Malyková D, Mattiello L, Pecinovská M, Petriščáková K, Průchová E, Stránská P, Smejtek L, Špaček J, Šumberová R, Švejcar O, Trefný M, Vávra M, Kolář J, Heyd V, Krause J, Pinhasi R, Reich D, Schiffels S, Haak W. Dynamic changes in genomic and social structures in third millennium BCE central Europe, *Sci. Adv*. **7** (2021) eabi6941. doi: 10.1126/sciadv.abi6941.

51. Patterson N, Price AL, Reich D. Population structure and eigenanalysis, *PLoS Genet*. **2** (2006) e190. doi: 10.1371/journal.pgen.0020190.

52. Patterson N, Moorjani P, Luo Y, Mallick S, Rohland N, Zhan Y, Genschoreck T, Webster T, Reich D. Ancient admixture in human history, Genetics. **192** (2012) 1065–1093. doi: 10.1534/genetics.112.145037.

53. Patterson N, Isakov M, Booth T, Büster L, Fischer CE, Olalde I, Ringbauer H, Akbari A, Cheronet O, Bleasdale M, Adamski N, Altena E, Bernardos R, Brace S, Broomandkhoshbacht N, Callan K, Candilio F, Culleton B, Curtis E, Demetz L, Carlson KSD, Edwards CJ, Fernandes DM, Foody MGB, Freilich S, Goodchild H, Kearns A, Lawson AM, Lazaridis I, Mah M, Mallick S, Mandl K, Micco A, Michel M, Morante GB, Oppenheimer J, Özdoğan KT, Qiu L, Schattke C, Stewardson K, Workman JN, Zalzala F, Zhang Z, Agustí B, Allen T, Almássy K, Amkreutz L, Ash A, Baillif-Ducros C, Barclay A, Bartosiewicz L, Baxter K, Bernert Z, Blažek J, Bodružić M, Boissinot P, Bonsall C, Bradley P, Brittain M, Brookes A, Brown F, Brown L, Brunning R, Budd C, Burmaz J, Canet S, Carnicero-Cáceres S, Čaušević-Bully M, Chamberlain A, Chauvin S, Clough S, Čondić N, Coppa A, Craig O, Črešnar M, Cummings V, Czifra S, Danielisová A, Daniels R, Davies A, de Jersey P, Deacon J, Deminger C, Ditchfield PW, Dizdar M, Dobeš M, Dobisíková M, Domboróczki L, Drinkall G, Đukić A, Ernée M, Evans C, Evans J, Fernández-Götz M, Filipović S, Fitzpatrick A, Fokkens H, Fowler C, Fox A, Gallina Z, Gamble M, González Morales MR, González-Rabanal B, Green A, Gyenesei K, Habermehl D, Hajdu T, Hamilton D, Harris J, Hayden C, Hendriks J, Hernu B, Hey G, Horňák M, Ilon G, Istvánovits E, Jones AM, Kavur MB, Kazek K, Kenyon RA, Khreisheh A, Kiss V, Kleijne J, Knight M, Kootker LM, Kovács PF, Kozubová A, Kulcsár G, Kulcsár V, Le Pennec C, Legge M, Leivers M, Loe L, López-Costas O, Lord T, Los D, Lyall J, Marín-Arroyo AB, Mason P, Matošević D, Maxted A, McIntyre L, McKinley J, McSweeney K, Meijlink B, Mende BG, Menđušić M, Metlička M, Meyer S, Mihovilić K, Milasinovic L, Minnitt S, Moore J, Morley G, Mullan G, Musilová M, Neil B, Nicholls R, Novak M, Pala M, Papworth M, Paresys C, Patten R, Perkić D, Pesti K, Petit A, Petriščáková K, Pichon C, Pickard C, Pilling Z, Price TD, Radović S, Redfern R, Resutík B, Rhodes DT, Richards MB, Roberts A, Roefstra J, Sankot P, Šefčáková A, Sheridan A, Skae S, Šmolíková M, Somogyi K, Somogyvári Á, Stephens M, Szabó G, Szécsényi-Nagy A, Szeniczey T, Tabor J, Tankó K, Maria CT, Terry R, Teržan B, Teschler-Nicola M, Torres-Martínez JF, Trapp J, Turle R, Ujvári F, van der Heiden M, Veleminsky P, Veselka B, Vytlačil Z, Waddington C, Ware P, Wilkinson P, Wilson L, Wiseman R, Young E, Zaninović J, Žitňan A, Lalueza-Fox C, de Knijff P, Barnes I, Halkon P, Thomas MG, Kennett DJ, Cunliffe B, Lillie M, Rohland N, Pinhasi R, Armit I, Reich D. Large-scale migration into Britain during the Middle to Late Bronze Age, *Nature*. **601** (2022) 588–594. doi: 10.1038/s41586-021-04287-4.

54. Peter BM. Admixture, Population Structure, and *F*-Statistics, *Genetics*. **202** (2016) 1485–1501. doi: 10.1534/genetics.115.183913.

55. Podani J, Miklós I. Resemblance coefficients and the horseshoe effect in Principal Coordinates Analysis, *Ecology*. **83** (2002) 3331–3343. doi: 10.1890/0012-9658(2002)083[3331:RCATHE]2.0.CO;2.

56. Prendergast ME, Lipson M, Sawchuk EA, Olalde I, Ogola CA, Rohland N, Sirak KA, Adamski N, Bernardos R, Broomandkhoshbacht N, Callan K, Culleton BJ, Eccles L, Harper TK, Lawson AM, Mah M, Oppenheimer J, Stewardson K, Zalzala F, Ambrose SH, Ayodo G, Gates HL Jr, Gidna AO, Katongo M, Kwekason A, Mabulla AZP, Mudenda GS, Ndiema EK, Nelson C, Robertshaw P, Kennett DJ, Manthi FK, Reich D. Ancient DNA reveals a multistep spread of the first herders into sub-Saharan Africa. *Science*. **365** (2019) eaaw6275. doi: 10.1126/science.aaw6275.
57. Raghavan M, Skoglund P, Graf KE, Metspalu M, Albrechtsen A, Moltke I, Rasmussen S, Stafford TW Jr, Orlando L, Metspalu E, Karmin M, Tambets K, Rootsi S, Mägi R, Campos PF, Balanovska E, Balanovsky O, Khusnutdinova E, Litvinov S, Osipova LP, Fedorova SA, Voevoda MI, DeGiorgio M, Sicheritz-Ponten T, Brunak S, Demeshchenko S, Kivisild T, Villems R, Nielsen R, Jakobsson M, Willerslev E. Upper Palaeolithic Siberian genome reveals dual ancestry of Native Americans. *Nature*. **505** (2014) 87–91. doi: 10.1038/nature12736.
58. Rasmussen M, Li Y, Lindgreen S, Pedersen JS, Albrechtsen A, Moltke I, Metspalu M, Metspalu E, Kivisild T, Gupta R, Bertalan M, Nielsen K, Gilbert MT, Wang Y, Raghavan M, Campos PF, Kamp HM, Wilson AS, Gledhill A, Tridico S, Bunce M, Lorenzen ED, Binladen J, Guo X, Zhao J, Zhang X, Zhang H, Li Z, Chen M, Orlando L, Kristiansen K, Bak M, Tommerup N, Bendixen C, Pierre TL, Grønnow B, Meldgaard M, Andreasen C, Fedorova SA, Osipova LP, Higham TF, Ramsey CB, Hansen TV, Nielsen FC, Crawford MH, Brunak S, Sicheritz-Pontén T, Villems R, Nielsen R, Krogh A, Wang J, Willerslev E. Ancient human genome sequence of an extinct Palaeo-Eskimo. *Nature*. **463** (2010) 757–762. doi: 10.1038/nature08835.
59. Reich D, Price AL, Patterson N. Principal component analysis of genetic data, *Nat. Genet*. **40** (2008) 491–492.
60. Reich D, Thangaraj K, Patterson N, Price AL, Singh L. Reconstructing Indian population history, *Nature*. **461** (2009) 489–494. doi: 10.1038/nature08365.
61. Reich D, Patterson N, Campbell D, Tandon A, Mazieres S, Ray N, Parra MV, Rojas W, Duque C, Mesa N, García LF, Triana O, Blair S, Maestre A, Dib JC, Bravi CM, Bailliet G, Corach D, Hünemeier T, Bortolini MC, Salzano FM, Petzl-Erler ML, Acuña-Alonzo V, Aguilar-Salinas C, Canizales-Quinteros S, Tusié-Luna T, Riba L, Rodríguez-Cruz M, Lopez-Alarcón M, Coral-Vazquez R, Canto-Cetina T, Silva-Zolezzi I, Fernandez-Lopez JC, Contreras AV, Jimenez-Sanchez G, Gómez-Vázquez MJ, Molina J, Carracedo A, Salas A, Gallo C, Poletti G, Witonsky DB, Alkorta-Aranburu G, Sukernik RI, Osipova L, Fedorova SA, Vasquez R, Villena M, Moreau C, Barrantes R, Pauls D, Excoffier L, Bedoya G, Rothhammer F, Dugoujon JM, Larrouy G, Klitz W, Labuda D, Kidd J, Kidd K, Di Rienzo A, Freimer NB, Price AL, Ruiz-Linares A. Reconstructing Native American population history, *Nature*. **488** (2012) 370–374. doi: 10.1038/nature11258.

62. Ringbauer H, Coop G, Barton NH. Inferring Recent Demography from Isolation by Distance of Long Shared Sequence Blocks, *Genetics*. **205** (2017) 1335–1351. doi: 10.1534/genetics.116.196220.
63. Scally A, Durbin R. Revising the human mutation rate: implications for understanding human evolution, *Nat. Rev. Genet*. **13** (2012) 745–753. doi: 10.1038/nrg3295.
64. Sirak KA, Fernandes DM, Lipson M, Mallick S, Mah M, Olalde I, Ringbauer H, Rohland N, Hadden CS, Harney É, Adamski N, Bernardos R, Broomandkhoshbacht N, Callan K, Ferry M, Lawson AM, Michel M, Oppenheimer J, Stewardson K, Zalzala F, Patterson N, Pinhasi R, Thompson JC, Van Gerven D, Reich D. Social stratification without genetic differentiation at the site of Kulubnarti in Christian Period Nubia, *Nat. Commun*. **12** (2021) 7283. doi: 10.1038/s41467-021-27356-8.
65. Skoglund P, Thompson JC, Prendergast ME, Mittnik A, Sirak K, Hajdinjak M, Salie T, Rohland N, Mallick S, Peltzer A, Heinze A, Olalde I, Ferry M, Harney E, Michel M, Stewardson K, Cerezo-Román JI, Chiumia C, Crowther A, Gomani-Chindebvu E, Gidna AO, Grillo KM, Helenius IT, Hellenthal G, Helm R, Horton M, López S, Mabulla AZP, Parkington J, Shipton C, Thomas MG, Tibesasa R, Welling M, Hayes VM, Kennett DJ, Ramesar R, Meyer M, Pääbo S, Patterson N, Morris AG, Boivin N, Pinhasi R, Krause J, Reich D. Reconstructing Prehistoric African Population Structure, *Cell*. **171** (2017) 59–71.e21. doi: 10.1016/j.cell.2017.08.049.
66. Soraggi S, Wiuf C. General theory for stochastic admixture graphs and *F*-statistics, *Theor. Popul. Biol*. **125** (2019) 56–66. doi: 10.1016/j.tpb.2018.12.002.
67. Taylor WTT, Librado P, American Horse CJ, Shield Chief Gover C, Arterberry J, Afraid of Bear-Cook AL, Left Heron H, Yellow Hair RM, Gonzalez M, Means B, High Crane S, Yellow Bull WW, Dull Knife B, Afraid of Bear A, Tecumseh Collin C, Ward C, Pasqual TA, Chauvey L, Tonasso-Calviere L, Schiavinato S, Seguin-Orlando A, Fages A, Khan N, Der Sarkissian C, Liu X, Wagner S, Leonard BG, Manzano BL, O'Malley N, Leonard JA, Bernáldez-Sánchez E, Barrey E, Charliquart L, Robbe E, Denoblet T, Gregersen K, Vershinina AO, Weinstock J, Rajić Šikanjić P, Mashkour M, Shingiray I, Aury JM, Perdereau A, Alquraishi S, Alfarhan AH, Al-Rasheid KAS, Trbojević Vukičević T, Buric M, Sauer E, Lucas M, Brenner-Coltrain J, Bozell JR, Thornhill CA, Monagle V, Perri A, Newton C, Hall WE, Conver JL, Le Roux P, Buckser SG, Gabe C, Belardi JB, Barrón-Ortiz CI, Hart IA, Ryder C, Sponheimer M, Shapiro B, Southon J, Hibbs J, Faulkner C, Outram A, Patterson Rosa L, Palermo K, Solé M, William A, McCrory W, Lindgren G, Brooks S, Eché C, Donnadieu C, Bouchez O, Wincker P, Hodgins G, Trabert S, Bethke B, Roberts P, Jones EL, Running Horse Collin Y, Orlando L. Early dispersal of domestic horses into the Great Plains and northern Rockies. *Science*. **379** (2023) 1316–1323. doi: 10.1126/science.adc9691.
68. Tricou T, Tannier E, de Vienne DM. Ghost Lineages Highly Influence the Interpretation of

Introgression Tests, *Syst. Biol*. **71** (2022) 1147–1158. doi: 10.1093/sysbio/syac011.

69. van de Loosdrecht M, Bouzouggar A, Humphrey L, Posth C, Barton N, Aximu-Petri A, Nickel B, Nagel S, Talbi EH, El Hajraoui MA, Amzazi S, Hublin JJ, Pääbo S, Schiffels S, Meyer M, Haak W, Jeong C, Krause J. Pleistocene North African genomes link Near Eastern and sub-Saharan African human populations. *Science*. **360** (2018) 548–552. doi: 10.1126/science.aar8380.

70. Wang K, Goldstein S, Bleasdale M, Clist B, Bostoen K, Bakwa-Lufu P, Buck LT, Crowther A, Dème A, McIntosh RJ, Mercader J, Ogola C, Power RC, Sawchuk E, Robertshaw P, Wilmsen EN, Petraglia M, Ndiema E, Manthi FK, Krause J, Roberts P, Boivin N, Schiffels S. Ancient genomes reveal complex patterns of population movement, interaction, and replacement in sub-Saharan Africa, *Sci. Adv*. **6** (2020) eaaz0183. doi: 10.1126/sciadv.aaz0183.

71. Wang CC, Yeh HY, Popov AN, Zhang HQ, Matsumura H, Sirak K, Cheronet O, Kovalev A, Rohland N, Kim AM, Mallick S, Bernardos R, Tumen D, Zhao J, Liu YC, Liu JY, Mah M, Wang K, Zhang Z, Adamski N, Broomandkhoshbacht N, Callan K, Candilio F, Carlson KSD, Culleton BJ, Eccles L, Freilich S, Keating D, Lawson AM, Mandl K, Michel M, Oppenheimer J, Özdoğan KT, Stewardson K, Wen S, Yan S, Zalzala F, Chuang R, Huang CJ, Looh H, Shiung CC, Nikitin YG, Tabarev AV, Tishkin AA, Lin S, Sun ZY, Wu XM, Yang TL, Hu X, Chen L, Du H, Bayarsaikhan J, Mijiddorj E, Erdenebaatar D, Iderkhangai TO, Myagmar E, Kanzawa-Kiriyama H, Nishino M, Shinoda KI, Shubina OA, Guo J, Cai W, Deng Q, Kang L, Li D, Li D, Lin R, Nini, Shrestha R, Wang LX, Wei L, Xie G, Yao H, Zhang M, He G, Yang X, Hu R, Robbeets M, Schiffels S, Kennett DJ, Jin L, Li H, Krause J, Pinhasi R, Reich D. Genomic insights into the formation of human populations in East Asia, *Nature*. **591** (2021) 413–419. doi: 10.1038/s41586-021-03336-2.

72. Yaka R, Mapelli I, Kaptan D, Doğu A, Chyleński M, Erdal ÖD, Koptekin D, Vural KB, Bayliss A, Mazzucato C, Fer E, Çokoğlu SS, Lagerholm VK, Krzewińska M, Karamurat C, Gemici HC, Sevkar A, Dağtaş ND, Kılınç GM, Adams D, Munters AR, Sağlıcan E, Milella M, Schotsmans EMJ, Yurtman E, Çetin M, Yorulmaz S, Altınışık NE, Ghalichi A, Juras A, Bilgin CC, Günther T, Storå J, Jakobsson M, de Kleijn M, Mustafaoğlu G, Fairbairn A, Pearson J, Togan İ, Kayacan N, Marciniak A, Larsen CS, Hodder I, Atakuman Ç, Pilloud M, Sürer E, Gerritsen F, Özbal R, Baird D, Erdal YS, Duru G, Özbaşaran M, Haddow SD, Knüsel CJ, Götherström A, Özer F, Somel M. Variable kinship patterns in Neolithic Anatolia revealed by ancient genomes. *Curr. Biol*. **31** (2021) 2455–2468.e18. doi: 10.1016/j.cub.2021.03.050.

73. Yang MA, Fan X, Sun B, Chen C, Lang J, Ko YC, Tsang CH, Chiu H, Wang T, Bao Q, Wu X, Hajdinjak M, Ko AM, Ding M, Cao P, Yang R, Liu F, Nickel B, Dai Q, Feng X, Zhang L, Sun C, Ning C, Zeng W, Zhao Y, Zhang M, Gao X, Cui Y, Reich D, Stoneking M, Fu Q. Ancient DNA indicates human population shifts and admixture in northern and southern China. *Science*. **369** (2020) 282–288.

doi: 10.1126/science.aba0909.

74. Zhang F, Ning C, Scott A, Fu Q, Bjørn R, Li W, Wei D, Wang W, Fan L, Abuduresule I, Hu X, Ruan Q, Niyazi A, Dong G, Cao P, Liu F, Dai Q, Feng X, Yang R, Tang Z, Ma P, Li C, Gao S, Xu Y, Wu S, Wen S, Zhu H, Zhou H, Robbeets M, Kumar V, Krause J, Warinner C, Jeong C, Cui Y. The genomic origins of the Bronze Age Tarim Basin mummies. *Nature*. **599** (2021) 256–261. doi: 10.1038/s41586-021-04052-7.